Progressive Low-Grade Metamorphism of a Black Shale Formation, Central Swiss Alps, with Special Reference to Pyrophyllite and Margarite Bearing Assemblages*

by MARTIN FREY†

Mineralogisch-petrographisches Institut der Universität Bern, Sahlistrasse 6, CH-3012 Bern, Switzerland

(*Received 23 July 1976, in revised form 21 February 1977*)

ABSTRACT

The unmetamorphosed equivalents of the regionally metamorphosed clays and marls that make up the Alpine Liassic black shale formation consist of illite, irregular mixed-layer illite/montmorillonite, chlorite, kaolinite, quartz, calcite, and dolomite, with accessory feldspars and organic material. At higher grade, in the anchizonal slates, pyrophyllite is present and is thought to have formed at the expense of kaolinite; paragonite and a mixed-layer paragonite/muscovite presumably formed from the mixed-layer illite/montmorillonite. Anchimetamorphic illite is poorer in Fe and Mg than at the diagenetic stage, having lost these elements during the formation of chlorite. Detrital feldspar has disappeared.

In epimetamorphic phyllites, chloritoid and margarite appear by the reactions pyrophyllite + chlorite = chloritoid + quartz + H_2O and pyrophyllite + calcite ± paragonite = margarite + quartz + H_2O + CO_2, respectively. At the epi–mesozone transition, paragonite and chloritoid seem to become incompatible in the presence of carbonates and yield the following breakdown products: plagioclase, margarite, clinozoisite (and minor zoisite), and biotite. The maximum distribution of margarite is at the epizone–mesozone boundary; at higher metamorphic grade margarite is consumed by a continuous reaction producing plagioclase.

Most of the observed assemblages in the anchi- and epizone can be treated in the two subsystems MgO (or FeO)–Na_2O–CaO–Al_2O_3–(KAl_3O_5–SiO_2–H_2O–CO_2). Chemographic analyses show that the variance of assemblages decreases with increasing metamorphic grade.

Physical conditions are estimated from calibrated mineral reactions and other petrographic data. The composition of the fluid phase was low in X_{CO_2} throughout the metamorphic profile, whereas X_{CH_4} was very high, particularly in the anchizone where a_{H_2O} was probably as low as 0·2. P–T conditions along the metamorphic profile are 1–2 kb/200–300 °C in the anchizone (Glarus Alps), and 5 kb/500–550 °C at the epi-mesozone transition (Lukmanier area). Calculated geothermal gradients decrease from 50 °C/km in the anchimetamorphic Glarus Alps to 30 °C/km at the epi-mesozone transition of the Lukmanier area.

INTRODUCTION

THE central Swiss Alps offer the rare opportunity to study specific lithostratigraphic units all the way from unmetamorphosed sediments to medium-grade metamorphic rocks. One such study, on a Triassic red bed formation has

* This paper is a condensed version of the author's 'Habilitationsschrift'.

† Present address: Mineralogisch-petrographisches Institut der Universität Basel, Bernoullistrasse 30, CH-4056 Basel, Switzerland.

already been documented (Frey, 1969*a*). The purpose of the present paper is to present complementary data on a related sequence of Liassic black shales.

Regional setting

The Liassic black shale formation studied was found at several localities: in the Jura mountains (the unmetamorphosed region), in the boreholes underneath the Molasse Basin and in the Helvetic Zone, and at the northern boundary of the Lepontine region (area of highest grade, see Fig. 1).

The unmetamorphosed clays and marls are exposed in the Tabular Jura of southern Germany and northwestern Switzerland, where they form part of the flat-lying foreland of the Alpine orogeny. The southern extension of the Tabular and Folded Jura has been found in several boreholes below the Molasse Basin to a depth of about 2 km (Büchi *et al.*, 1965).

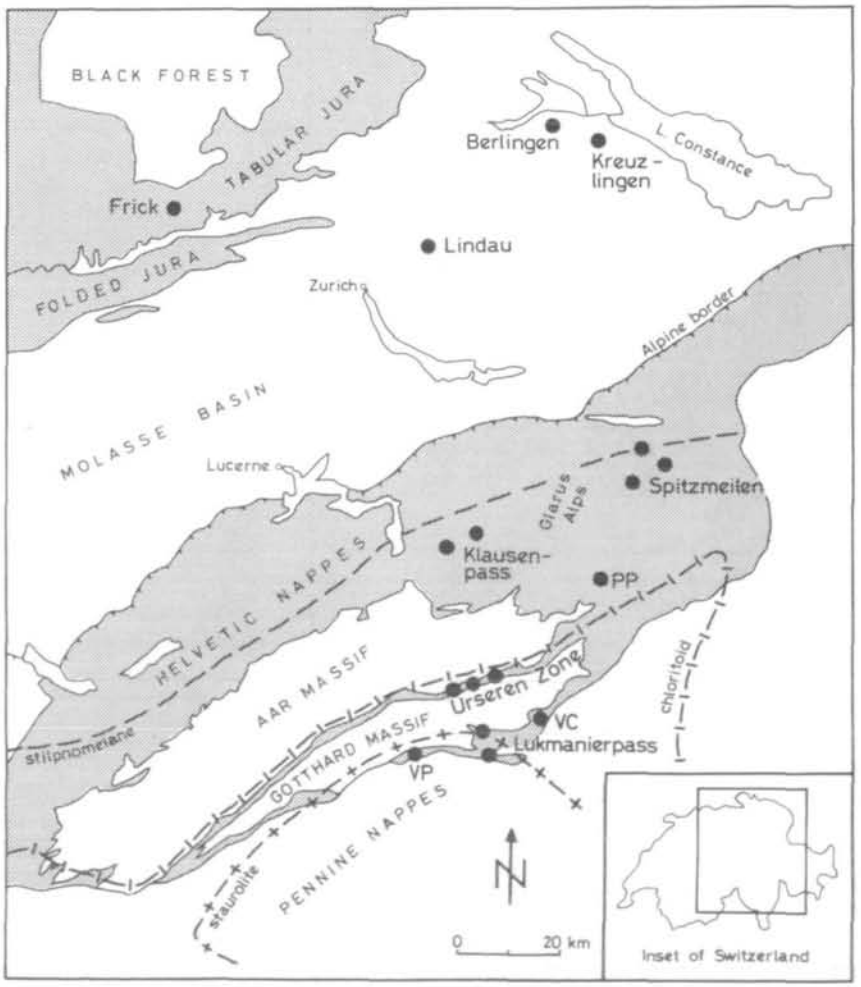

FIG. 1. Simplified geologic map of the central Swiss Alps showing main sample localities (black dots). Stippled areas: Jura and Helvetic domains. Metamorphic mineral zone boundaries after Niggli & Niggli (1965) with minor modifications. Abbreviations for localities: PP = Panixerpass; VC = Valle Cavalasca; VP = Val Piora.

The anchimetamorphic shales and slates of this formation (the anchizone being defined on the basis of illite crystallinity—Kübler, 1967) are found in the Helvetic Nappes, which form the Alpine border region of central Switzerland. The Helvetic Nappes consist mainly of miogeosynclinal sediments which slid northwards off the Aar and Gotthard Massifs in great recumbent folds and thrust slices (Trümpy, 1960). Until recently, the Helvetic Nappes were considered unmetamorphosed.

The epi- and mesometamorphic phyllites and schists belong to the northern and southern sedimentary cover of the Gotthard Massif, respectively. The Gotthard Massif itself lies within the chloritoid zone of Alpine metamorphism as defined by Niggli & Niggli (1965).

Stratigraphy

The Liassic rocks of the Jura mountains consist of 20–60 m of grey to black clays, marls, sandstones and arenaceous limestones (Heim, 1919). In the Glarus Alps, these rocks reach a thickness of 350–500 m (Trümpy, 1949). At its base, the Liassic sequence is composed of 30 m of sandstones with intercalated black shales and slates (= member I in Fig. 5). Overlying rock units (= member II and III in Fig. 5) consist of 100–150 m of grey to black marly shales and slates with intercalations of arenaceous limestones. The rocks which in turn overlie these marly shales and slates are mainly arenaceous limestones and were excluded from this study. Further south, in the Urseren Zone, the Liassic rocks consist of 50–70 m of black to grey phyllites and schists with intercalated arenaceous limestones at the base (= members I?, II and III in Fig. 7), and 40–80 m of arenaceous limestones at the top (= member IV in Fig. 7—see Niggli, 1944). At the Lukmanier Pass these Liassic sediments are at least 700 m thick and consist of a basal 10 m of pelitic black schists with minor quartzites (= members I and II in Fig. 9), overlain by 50 m of alternating marly black schists and limestones (= member III in Fig. 9). Only the lower Liassic of the Lukmanier area has low-grade equivalents in the Urseren Zone and the Glarus Alps (Baumer *et al.*, 1961; Frey, 1967).

METHODS

Sampling procedure. Whenever possible, complete stratigraphic sections were sampled taking into account all lithological variations. At most localities 10 to 25 specimens were collected at intervals of decimeters to several meters.

Mineral identification. For the unmetamorphosed and metamorphosed sediments of the anchizone, mineral determinations were obtained primarily by X-ray studies. In all other cases, combinations of optical and X-ray methods were applied. The identification of the sheet silicates, including the clay minerals, was made by X-ray diffractometer and Guinier camera techniques. The X-ray mounts were prepared by sedimentation, and were air-dried, glycolated or heat treated where necessary. Accurate determinations of d-spacings were obtained using Si or quartz as internal standards.

Modal analysis. Quantitative determination of quartz and feldspars was done by X-ray analysis, using a method devised by Peters (1965, 1970). The amounts of the various carbonate minerals were calculated from the known calcite/dolomite ratio

coupled with volumetrically determined CO_2 values in the bulk samples. Sheet silicate abundance could only be determined semiquantitatively by X-ray diffractometry; the method used was that outlined by Henderson (1971). In all cases, the X-ray standards used were prepared by mechanically mixing equal amounts of various combinations of minerals, followed by measurements of the intensity ratios of the reflexions indicated in Table 1.

TABLE 1

Intensity-ratios used for semiquantitative determination of sheet silicates. The ratios shown result from equal proportions of the minerals listed

A			*B*			*A:B*
Mineral	*h k l*	*d in Å*	*Mineral*	*h k l*	*d in Å*	*Intensity ratio*
Illite	0 0 1	10	Montmorillonite	0 0 1	17	1:3
Illite	0 0 1	10	Chlorite	0 0 2	7	1:2
Illite	0 0 1	10	Kaolinite	0 0 2	3·60	1:2
Chlorite	0 0 4	3·56	Kaolinite	0 0 2	3·60	1:1
Muscovite	0 0 2	10	Pyrophyllite	0 0 1	9·2	1:1
Muscovite	0 0 6	3·3	Paragonite	0 0 6	3·20	1:1
Muscovite	0 0 6	3·3	Paragonite/muscovite	—	3·25	1:1
Muscovite	0 0 2	10	Margarite	0 0 2	9·6	7:1
Muscovite	0 0 6	3·3	Margarite	0 0 6	3·2	1:1
Muscovite	0 0 . 10	2·0	Margarite	0 0 . 10	1·91	5:4
Margarite	0 0 . 10	2·0	Paragonite	0 0 . 10	1·92	4:5
Muscovite	0 6 0	1·50	Paragonite	0 6 0	1·48	1:1
Muscovite	0 6 0	1·50	Margarite	0 6 0	1·47	1:1

Chemical and microprobe analyses. Whole rock analyses were done by standard wet chemical methods. Some of the mineral analyses were performed at Cambridge University by J. S. Fox on a Geoscan electron-probe microanalyser, using simple silicates and oxides as standards. Corrections were done according to the procedure described by Sweatman & Long (1969). The remaining analyses were carried out by the author on an Acton–Cameca electron-probe at Yale University using standards with a composition close to that of the unknown mineral. In this case, corrections were made with the method of Bence & Albee (1968).

Where minerals were too fine-grained to be analysed satisfactorily by microprobe, their chemical compositions were estimated from X-ray data.

MINERAL COMPOSITIONS AND ABBREVIATIONS

The compositions of the phases based on which the stoichiometry of the reactions were calculated and the abbreviations for mineral names used in the tables and figures are listed below:

ab = albite, $NaAlSi_3O_8$
cc = calcite, $CaCO_3$
chl = chlorite, $(Fe,Mg)_{4\cdot5}Al_3Si_{2\cdot5}O_{10}(OH)_8$

ctd	= chloritoid,	$FeAl_2SiO_5(OH)_2$
dol	= dolomite,	$CaMg(CO_3)_2$
ma	= margarite,	$CaAl_4Si_2O_{10}(OH)_2$
pa	= paragonite,	$NaAl_3Si_3O_{10}(OH)_2$
py	= pyrophyllite,	$Al_2Si_4O_{10}(OH)_2$
zo	= zoisite,	$Ca_2Al_3Si_3O_{12}(OH)$

bi	= biotite	kf	= K-feldspar
clz	= clinozoisite	ky	= kyanite
c/m	= chlorite/montmorillonite mixed-layer	mu	= muscovite
gr	= garnet	pa/mu	= paragonite/muscovite mixed-layer
i	= illite	plag	= plagioclase
i/m	= illite/montmorillonite mixed-layer	rect	= rectorite
kaol	= kaolinite	st	= staurolite

BULK ROCK CHEMISTRY

To test for isochemistry in the formation, composite rock samples were analysed from all the four areas under consideration. As can be seen from Table 2, the mean rock compositions are similar in all four areas, although the chemical diversity in a single outcrop may be considerable (see below) with the largest variations due to the changing carbonate content.

MINERALOGY AND PETROGRAPHY

The unmetamorphosed marls and claystones of the Tabular Jura and the boreholes under the Molasse Basin

The unmetamorphosed Liassic rocks from under the Molasse Basin were studied using drill hole samples from the Berlingen, Kreuzlingen and Lindau localities (see Fig. 1). Additional data by Peters (1964) was available from the Frick area. In all, a total of 34 samples were investigated.

Mineralogy

Illite and irregular mixed-layer illite/montmorillonite. Illite was determined by its strong basal reflexions at 10 Å and 5 Å. Diffractograms of the air-dried mixed-layer illite/montmorillonite showed a broad basal reflexion at about 10–13 Å. On glycolation, this reflexion shifted to roughly 12–14 Å, indicating the presence of 20–40 per cent expandable layers (MacEwan *et al.*, 1961, fig. XI. 17). Absence of a regular sequence of higher and lower order basal reflexions indicated a random interstratification of illite and montmorillonite. The (060)-reflexion varied from 1·498 to 1·504 Å, indicating up to 25 per cent Mg and Fe in the octahedral layer (Maxwell & Hower, 1967, fig. 4).

Chlorite. The first five basal reflexions appeared on X-ray diffractograms. In six

TABLE 2

Composite analyses of Liassic sediments from different outcrop areas

Wt. %	*Boreholes m = 24*	*Glarus Alps m = 74*	*Urseren Zone m = 58*	*Lukmanier area m = 18*	*Pelitic rocks n = 155 (Shaw, 1956)*	*Shales from platforms n = 6800 (Vinogradov & Ronov, 1956)*	*Black shales n = 779 (Vine & Tourtelot, 1970)*	*Lower Liassic Metapelites Lukmanier area n = 14 (Fox, 1974)*
SiO_2	58·2	56·5	59·0	54·4	61·54	50·7	n.d.	59·09
TiO_2	0·55	0·64	0·64	0·80	0·82	0·78	0·33	1·51
Al_2O_3	13·2	18·4	18·6	16·8	16·95	15·1	13·23	26·54
FeO*	4·0	4·2	5·5	4·3	6·21	6·3	2·58	5·36
MnO	0·04	0·04	0·05	0·06	n.d.	0·08	0·02	0·04
MgO	1·8	1·4	1·5	1·8	2·52	3·3	1·16	1·40
CaO	6·1	4·2	2·9	7·3	1·76	7·2	2·10	0·54
Na_2O	0·7	1·2	0·9	0·8	1·84	0·8	0·94	1·31
K_2O	3·5	3·6	3·6	4·6	3·45	3·5	2·41	2·90
P_2O_5	0·07	0·12	0·19	0·13	n.d.	0·10	n.d.	n.d.
H_2O_{tot}	5·0	4·5	3·5	1·3	3·47	5·0	n.d.	n.d.
CO_2	6·4	3·9	2·8	6·9	1·67	6·1	1·21	n.d.
C	0·61	0·47	0·53	0·40	n.d.	0·67	3·2	n.d.
S	1·1	0·19	0·18	0·28	n.d.	n.d.	n.d.	n.d.
Total	101·27	99·36	99·89	99·87	100·23	99·55	—	98·69

* Total Fe as FeO. n.d. = not determined.

For locations see Fig. 1. Analyst M. Frey. In this work, several powdered samples (number = *m*) were physically mixed and analysed. The average analyses from other work (number = *n*) are shown for comparison.

samples, the position of the first basal reflexion, calculated from $d(004)$, ranged between 14·12 to 14·17 Å. The b parameter, calculated from the (060)-reflexion, varied in four samples from 9·29 to 9·30 Å. According to Wetzel (1973, table 3) these values correspond to the following structural formula:

$$(Mg_{2.4-2.3}Fe^{2+}_{2.3-2.6}Al_{1.3-1.1})_6(Si_{2.7_5-2.8_5}Al_{1.2_5-1.1_5})_4O_{10}(OH)_8$$

Peak intensities before and after heat treatment also indicate a relatively Fe-rich chlorite.

Mixed-layer chlorite/montmorillonite. A broad basal reflexion at 13·5–14·1 Å, found only in air-dried samples, indicated an additional phase in these unmetamorphosed assemblages. The glycolated diffractogram showed a more or less regular sequence of basal reflexions. The $d(001)$ value, as obtained from the $d(00.10)$ reflexion, is 34·5 Å. On heat treatment, a broad but weak shoulder appears at about 11–12·6 Å. In most samples only this weak shoulder (see Fig. 2)

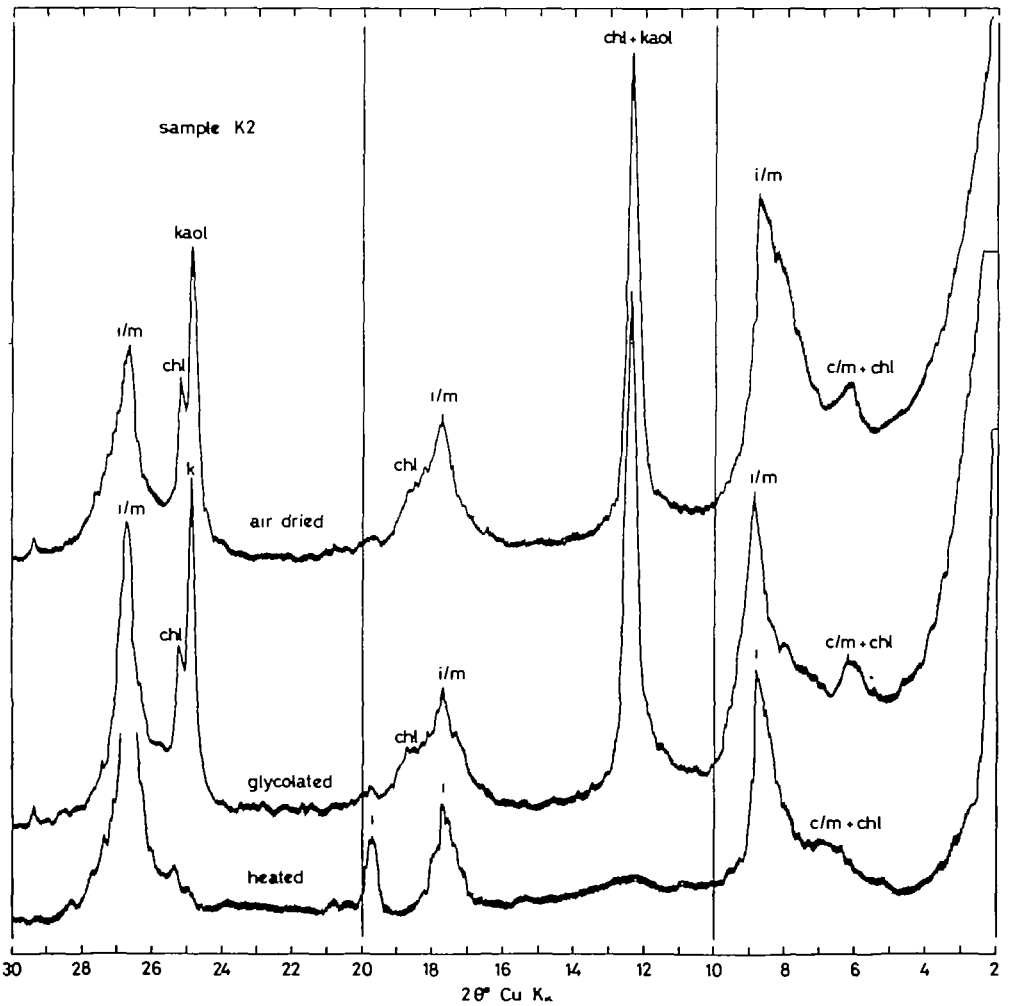

FIG. 2. Diffractograms of the unmetamorphosed sample K2 from the Kreuzlingen borehole. All fractions <2 μ. For mineral abbreviations refer to p. 98.

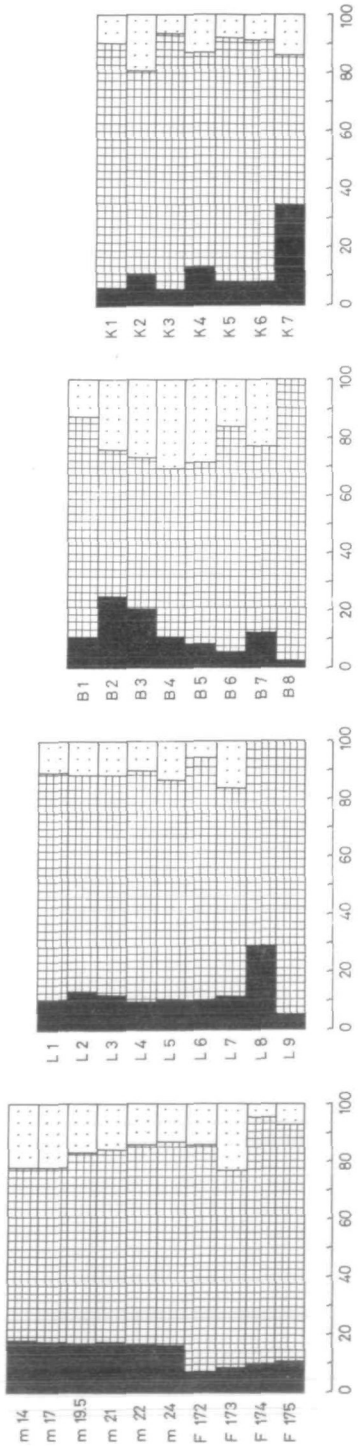

FIG. 3. Clay mineral distribution (fraction $<2\,\mu$) for the unmetamorphosed Liassic at Frick (Tabular Jura) and three boreholes under the Molasse Basin.

points to the presence of this clay mineral which is interpreted as a 1/1 chlorite/montmorillonite interstratification with a tendency to regular ordering. A similar clay mineral was described by Tank & McNeely (1970) from epigenetic graywackes.

Kaolinite. The first basal reflexion of kaolinite coincided with the (002)-reflexion of chlorite; but the second order basal reflexion at 3·60 Å was resolved from the (004)-reflexion of chlorite at 3·56 Å by using a slow scanning speed. Sharp lines on Guinier films indicated significant layer ordering.

In addition to the clay minerals in all samples studied, the *other phases* included quartz, calcite, minor dolomite, feldspars (albite and K-feldspar), and accessory pyrite, anatase and organic material.

Modal and bulk rock composition

A typical diffractogram of the clay fraction of an unmetamorphic Liassic marl is given in Fig. 2. The clay mineral distribution of the $<2\,\mu$ fraction of all investigated

TABLE 3

Modal and bulk rock composition of three representative unmetamorphosed samples

	*m14**	*B3*	*K2*	*Average of 24 samples*
Illite & illite/montm.	25	45–50	40	
Chlorite	5–10	<5	5	
Chlorite/montm.	—	≪5	≪5	
Kaolinite	10	5–10	10	
Quartz	33	23	42	
k-feldspar	4	2½	—	
Albite	3½	—	3	
Calcite	18	13½	½	
Dolomite	—	2½	—	
SiO_2	59·7	47·5	62·6	58·2
TiO_2	0·69	0·67	0·99	0·55
Al_2O_3	10·5	17·4	18·3	13·2
FeO†	2·2	4·8	4·0	4·0
MnO	0·02	0·07	0·01	0·04
MgO	1·8	1·7	1·2	1·8
CaO	10·5	8·6	0·53	6·1
Na_2O	0·54	0·8	0·8	0·7
K_2O	2·3	4·1	3·5	3·5
P_2O_5	0·07	0·10	0·04	0·07
H_2O_{tot}	2·7	6·4	5·9	5·0
CO_2	7·9	7·1	0·21	6·4
C	0·70	0·95	0·87	0·61
S	n.d.	n.d.	n.d.	1·1
Total	99·62	100·37	98·95	101·27

* Analysis m14 of the decarbonated host rock (Peters, 1964, table 8) recalculated for a calcite content of 18 wt. per cent of ideal composition.

† Total Fe as FeO.

Analysts M. Frey and T. Peters (m14). The average chemical composition of 24 unmetamorphosed marls and claystones from Table 1 is reproduced for comparison. All values in wt. per cent.

samples is shown in Fig. 3. Illite and an irregular mixed-layer illite/montmorillonite are the dominant clay minerals (50–95 per cent); chlorite (<5–30 per cent) is seen to occur in all samples. Although not shown in Fig. 3, the mixed-layer chlorite/montmorillonite (<5 per cent) is present in all samples except K5. Kaolinite (5–30 per cent) is the characteristic clay mineral in all four sections studied.

Table 3 gives modal and bulk rock compositions of three representative rocks. A comparison of these data leads to the conclusion that most of the sodium must be incorporated in the illite or the mixed-layer illite/montmorillonite. The same is true for the iron, and to a lesser extent for the magnesium. This is in accordance with the X-ray data mentioned earlier. Table 4 lists the mineral assemblages observed in 34 unmetamorphosed sedimentary rocks.

TABLE 4

Mineral assemblages in 34 unmetamorphic Liassic samples of the Tabular Jura and of boreholes below the Molasse Basin

i + i/m	*chl*	*kaol*	*cc*	*dol*	*ab*	*kf*	*Number of samples*
×	×	×	×		×	×	9
×	×	×	×		×		5
×	×	×	×				4
×	×	×	×	×			4
×	×	×	×	×	×		2
×	×	×	×	×	×	×	2
×	×	×					2
×	×	×				×	1
×	×	×			×	×	1
×	×	×		×		×	1
×	×		×	×	×		2
×	×		×		×		1
34	34	31	29	11	22	14	34

Quartz and organic material are always present in addition.

The anchimetamorphosed shales and slates of the Glarus Alps

109 anchimetamorphic, Lower Liassic shale and slate samples, from the Glarus Alps were studied. All samples were taken from sections described by Trümpy (1949) and were mainly from the Spitzmeilen and the Klausenpass regions (see Fig. 1).

Mineralogy

Muscovite–illite. A dioctahedral phyllosilicate, whose 10 Å basal reflexion was not affected by glycol treatment, was called 'muscovite–illite'. Additional properties of this phase were found to be: (i) a better crystallinity than the illites from the Molasse Basin borehole samples; (ii) a gradual elimination of interlayer vacancies with increasing grade; (iii) a strong maximum at 1·498 Å in the frequency distribution of $d(060)$ values, as compared with a 1·4988 ± 0·0002 Å mode for

synthetic $2M_1$ muscovite (Chatterjee & Johannes, 1974), indicating a negligible phengite miscibility.

The crystallinity of illite was determined only rarely because its first order basal reflexion was found to interfere with that of pyrophyllite, paragonite, and mixed-layer paragonite/muscovite. When measurable, this value ranged between 5 and 7 for the Spitzmeilen region and around 5 for the Klausenpass area*.

Basal spacings of muscovites which coexist with paragonite indicated 2–6 mole per cent paragonite solid solution, according to a relation given by Guidotti (1974).

Chlorite. A first approximation to the chlorite composition was obtained by X-ray studies. According to Wetzel (1973) determination of the b parameter and the $c.\sin\beta$ spacing permits an estimation of x and y values in the chlorite formula $(Mg_{6-x-y}Fe^{2+}_yAl_x)_6(Si_{4-x}Al_x)_4O_{10}(OH)_8$. In 28 samples, the $d(001)$ value varied between 14·09 and 14·14 Å, with an average around 14·11–14·12 Å, corresponding to a mean x value of 1·35. In 68 samples the b parameter varied between 9·24 and 9·32 Å, with an average around 9·29 Å, leading to a y value of 2·3. Accordingly, most of the anchimetamorphic chlorites may approximate to the following structural formula:

$$(Mg_{2\cdot3_5}Fe^{2+}_{2\cdot3}Al_{1\cdot3_5})_6(Si_{2\cdot7}Al_{1\cdot3})_4O_{10}(OH)_8$$

and should be termed 'ripidolite' (Hey, 1954). It should be pointed out that the regression formulae used were derived from relatively high-temperature chlorites and that the compositions of the low-temperature chlorites deduced from these formulae may be inaccurate.

7 Å-chamosite. A 7 Å-chamosite with $d(001) = 7{\cdot}07$ Å and $b = 9{\cdot}31_7$ Å was identified with certainty only in a few samples, these being from the Triassic–Liassic transition zone of the Spitzmeilen region. After heat treatment (1100 °C for 2 hours in air) hematite and spinel—but no olivine—were found, indicating that these are true chamosites (Warshaw & Roy, 1961). The 7 Å-chamosite is probably more common in these rocks, but it is difficult to detect it in the presence of 14 Å-chlorite.

Rectorite (?). Some samples at the low-grade end of the anchizone contain minor amounts of an expanding clay mineral with a first order basal reflexion between 22–23 Å for air-dried, and 25–27 Å for glycolated samples. Higher order reflexions are apparently missing. This phase may be rectorite, $Na_xAl_2\,[Si_{4-x}Al_xO_{10}]\,(OH)_2$.

Mixed-layer paragonite/muscovite. This mineral was first described by Frey (1969*b*), who found it in the anchimetamorphosed shales and slates of the Glarus Alps. A strong basal reflexion at 3·25 Å and a weaker one at 1·96 Å are characteristic of this mineral.

Paragonite. Paragonite was identified by its first three basal reflexions and was distinguished from margarite through the measurement of the (00.10) basal reflexion.

Pyrophyllite. Pyrophyllite is easily detected by its basal reflexions at 9·2, 4·6 and 3·06 Å and is distinguished from talc by its (060)-reflexion at 1·49 Å. Using the method of Brindley & Wardle (1970), the triclinic pyrophyllite was found to

* The illite crystallinity for anchimetamorphic rocks in general ranges from 7·5 to 4·0.

predominate over the monoclinic form in the anchizone rocks. The third basal spacings of samples MF 537 and MF 702 (Table 5) were found to be 3·066 ± 0·001 and 3·065 ± 0·001 Å, respectively. These values are similar to those of other natural pyrophyllites but appreciably smaller than those of synthetic pyrophyllites (Rosenberg, 1974, fig. 1). Occasionally, rims of a sheet silicate mineral with low birefringence, probably secondary pyrophyllite, were observed on grains of detrital muscovite (cf. Chennaux & Dunoyer, 1967).

The *other main phases* in all anchizone samples are quartz, ferroan calcite and ferroan dolomite as revealed by staining methods (Dickson, 1966). No feldspar was detected in any of the shales and slates, although minor detrital feldspar is reported from the intercalated quartzites (Trümpy, 1949). The most frequent *accessory minerals* are pyrite, tourmaline and organic material (graphite d_3, Landis, 1971).

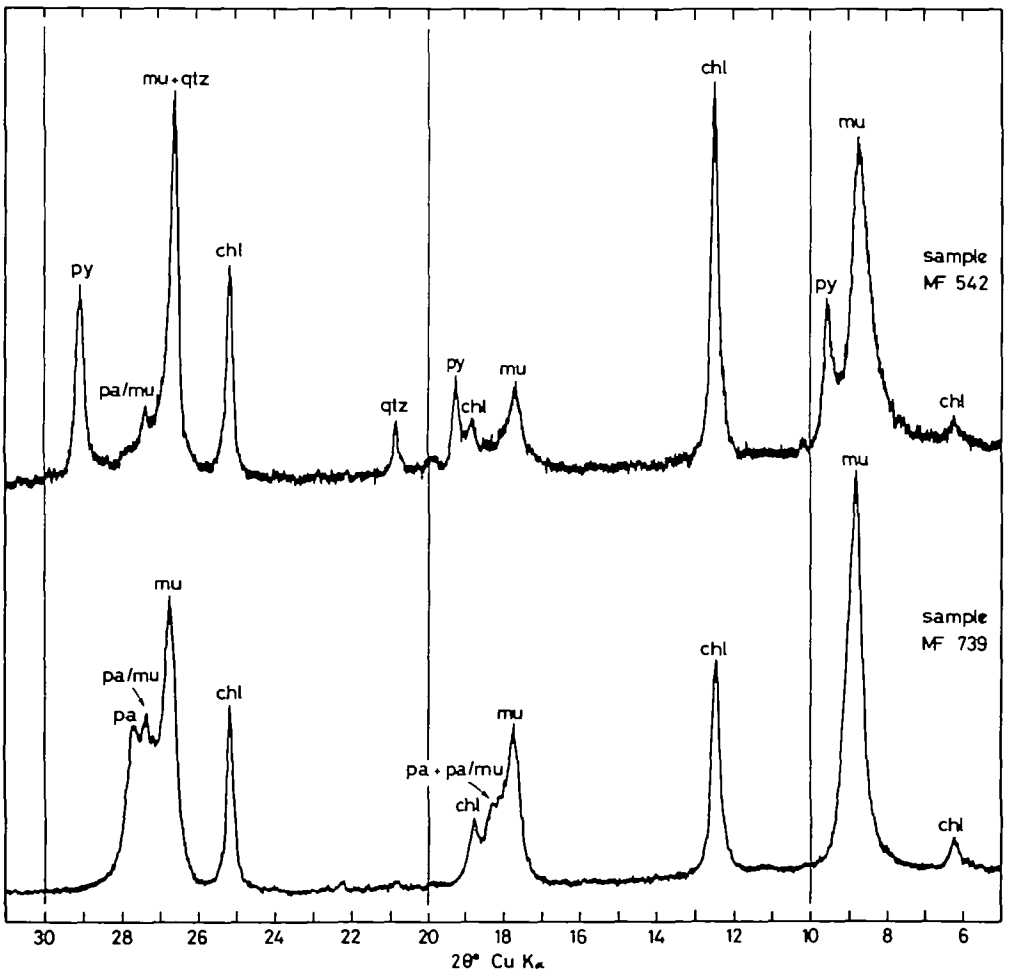

FIG. 4. Diffractograms of two typical anchimetamorphic samples from the Glarus Alps (fraction <2 μ). For mineral abbreviations refer to p. 98.

Modal and bulk rock composition

Typical diffractograms of the clay fraction of two anchimetamorphic Liassic shales are shown in Fig. 4. The sheet silicate distributions of the $<2\mu$ fraction of four out of ten sections studied are shown in Fig. 5. Muscovite–illite is the dominant sheet silicate (10–95 per cent) but chlorite (5–60 per cent) also occurs in all samples. Paragonite (0–25 per cent) and/or mixed-layer paragonite/muscovite

TABLE 5

Modal and bulk rock composition of six anchimetamorphic samples (extreme types) of the Glarus Alps

	MF 537	*MF 551*	*MF 561*	*MF 626*	*MF 644*	*MF 702*	*Average of 74 samples*
Muscovite–illite	10–15	15–20	35–40	10–15	15	10	
Chlorite	5	20	5	25	<5	<5	
Paragonite/muscovite	5	+?	15–20	+?	10–15	5	
Paragonite	—	—	15	+?	5–10	—	
Pyrophyllite	50–55	—	—	—	—	70	
Quartz	20	58	25	47	60	14	
Calcite	—	1½	—	14	—	—	
Dolomite	4	—	—	1	—	—	
SiO_2	60·6	72·1	59·3	58·9	78·1	58·9	56·5
TiO_2	1·3	0·56	1·1	0·49	0·47	1·2	0·64
Al_2O_3	23·8	10·8	24·2	10·3	11·6	28·0	18·4
FeO*	2·3	7·7	1·5	8·3	0·80	1·6	4·2
MnO	0·02	0·01	<0·01	0·14	<0·01	<0·01	0·04
MgO	1·0	1·5	1·1	3·5	0·4	0·24	1·4
CaO	1·5	0·89	0·21	7·5	0·06	0·03	4·2
Na_2O	0·25	0·10	1·5	0·23	0·6	0·60	1·2
K_2O	1·5	1·9	5·9	0·9	1·4	1·6	3·6
P_2O_5	0·04	0·16	0·04	0·09	0·13	0·04	0·12
H_2O^+	4·4	3·3†	4·0	4·1†	2·6	5·5	4·5†
H_2O^-	0·21		1·1		0·8	0·24	
CO_2	1·9	0·58	–	6·2	—	—	3·9
C	0·19	0·44	0·28	0·07	1·4	0·32	0·47
S	n.d.	n.d.	n.d.	n.d.	n.d.	n.d.	0·19
Total	99·01	100·04	100·23	100·72	98·36	98·27	99·36

* Total Fe as FeO. †H_2O_{tot}.

Analyst M. Frey. The average chemical composition of 74 anchimetamorphic shales and slates from Table 1 is shown for comparison. All values in wt. per cent.

(0–25 per cent) is very common; paragonite was detected with certainty in 44 and the mixed-layer paragonite/muscovite in 99, out of 109 samples (Table 6). The mixed-layer paragonite/muscovite often dominates over paragonite (Fig. 5). Pyrophyllite (0–75 per cent) is a characteristic sheet silicate in 47 out of 109 samples.

Table 5 gives the mineralogical and chemical composition of six rocks. Extreme types were chosen to set upper limits for the modal contents of chlorite (samples MF 551 and 626), paragonite, mixed-layer paragonite/muscovite (samples MF 561 and 644) and pyrophyllite (samples MF 537 and 702).

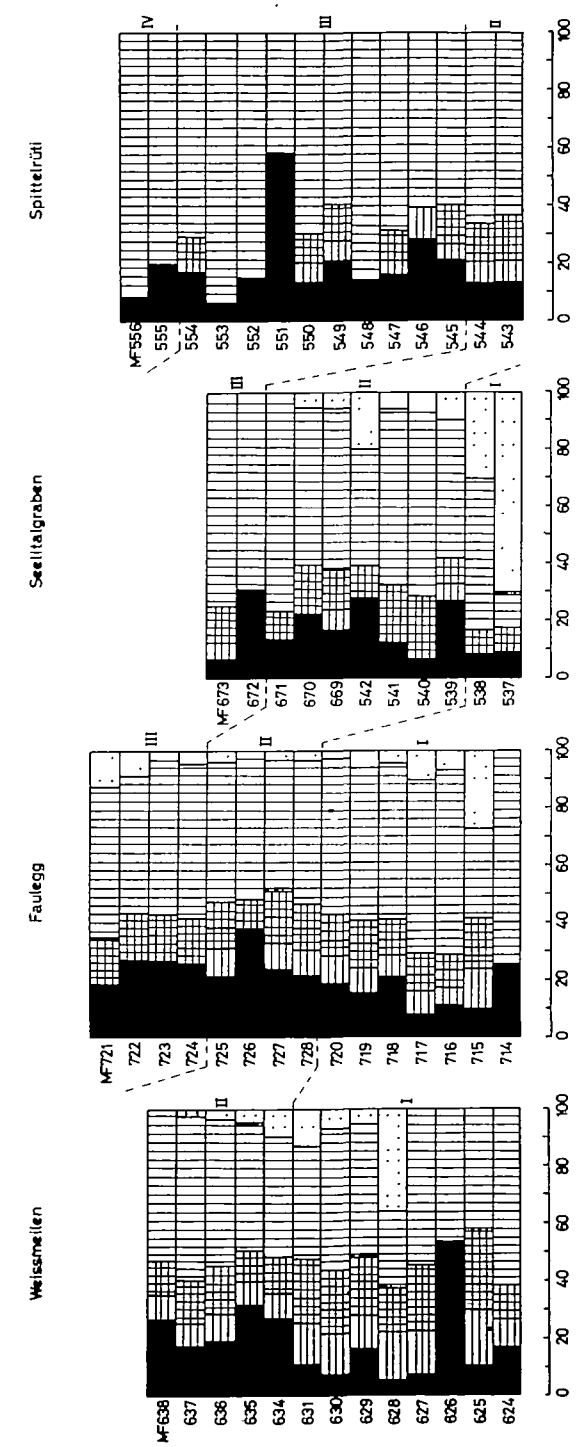

FIG. 5. Sheet silicate distribution (fraction $<2\ \mu$) in four stratigraphic sections from the Glarus Alps. Weissmeilen and Faulegg are located in the Spitzmeilen area (Fig. 1), Seelitalgraben and Spittelrüti in the Klausenpass area. I–IV designate lithostratigraphic units (members) within the Liassic of the Glarus Alps after Trümpy (1949): I = Infralias, II = Cardinienschichten, III = Prodkammserie, IV = Spitzmeilenserie.

Table 6 lists the mineral assemblages observed in 109 anchimetamorphic samples of the Glarus Alps. Note the common occurrence of the assemblages containing the sheet silicates pyrophyllite, mixed-layer paragonite/muscovite, paragonite, and the carbonate minerals, the significance of which will be discussed later.

TABLE 6

Mineral assemblages in 109 anchimetamorphic shales and slates of the Glarus Alps

mu-i	*chl*	*py*	*rect*	*pa/mu*	*pa*	*cc*	*dol*	*Number of samples*
×	×	×		×	×			23
×	×	×		×	+?			6
×	×	×		×	+?	×		6
×	×	×		×				4
×	×	×		×	×	×		2
×	×	×		×		×		2
×	×	×		×	×	×	×	1
×	×	×		×	+?	×	×	2
×	×	×		×		×	×	1
×	×		×	×	+?	×	×	2
×	×		×	×	+?	×		1
×	×		×			×	×	1
×	×			×	×			13
×	×			×	+?	×		9
×	×			×	+?			7
×	×			×	×	×		5
×	×					×		5
×	×			×				4
×	×							4
×	×			×		×		4
×	×			×		×	×	4
×	×			×	+?	×	×	3
109	109	47	4	99	44 + 36?	46	14	109

Quartz and organic material are always present in addition.

The epimetamorphic phyllites and schists of the Urseren Zone

77 epimetamorphic phyllites and schists, mainly from three sections of Lower Liassic rocks from the Urseren Zone, were studied.

Mineralogy

Muscovite. As in the Glarus Alps, the maximum at 1·498 Å in the frequency distribution of $d(060)$ values indicated that the muscovites of the Urseren Zone contain only negligible amounts of phengitic component. These phengite-poor K-micas may be a result of highly aluminous rock compositions (Guidotti & Sassi, 1976).

As before, basal spacings of some coexisting muscovites and paragonites were measured; these indicated 8–11 mole per cent paragonite in muscovite.

The 'illite crystallinity' (Kübler, 1967) of all samples free of paragonite and/or margarite is <4·0, indicative of epizonal conditions.

Chlorite. The chlorite composition was determined by the X-ray method described earlier. On the basis of some 20 measurements, the epimetamorphic chlorites of the Urseren Zone were estimated to have the following structural formula (Wetzel, 1973):

$$(Mg_{2.4-2.9}, Fe^{2+}_{2.3-1.7})Al_{1.3})_6(Si_{2.7}Al_{1.3})_4O_{10}(OH)_8$$

Again, these chlorites fall in the ripidolite field as defined by Hey (1954).

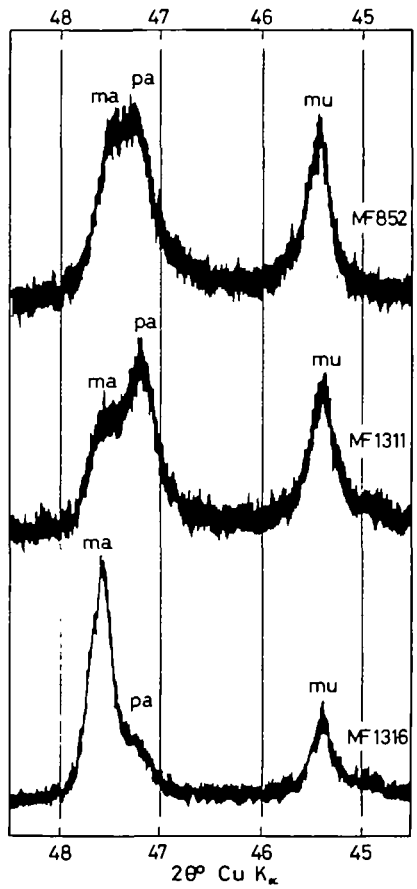

FIG. 6. Diffractometer traces for three samples containing muscovite, paragonite, and margarite in different proportions. The 2θ range shown is critical for the distinction between the three white micas.

Mixed-layer paragonite/muscovite. The X-ray properties of this phase do not appear to have changed in comparison with its anchizone equivalent.

Paragonite. The $d(002)$ spacings of some paragonites of the Urseren Zone were found to be lower than that of a synthetic $2M_1$ paragonite (Chatterjee, 1974*a*). This might imply some solid solution of margarite in these paragonites.

Margarite. In fine grained phyllites, margarite can be detected unequivocally only by X-ray methods. There are three different ways of distinguishing margarite from paragonite: (i) From the position of the (00.10) basal reflexion (Chatterjee, 1971, p. 193), see Fig. 6; (ii) from its (060) reflexion (Velde, 1971); and (iii) from

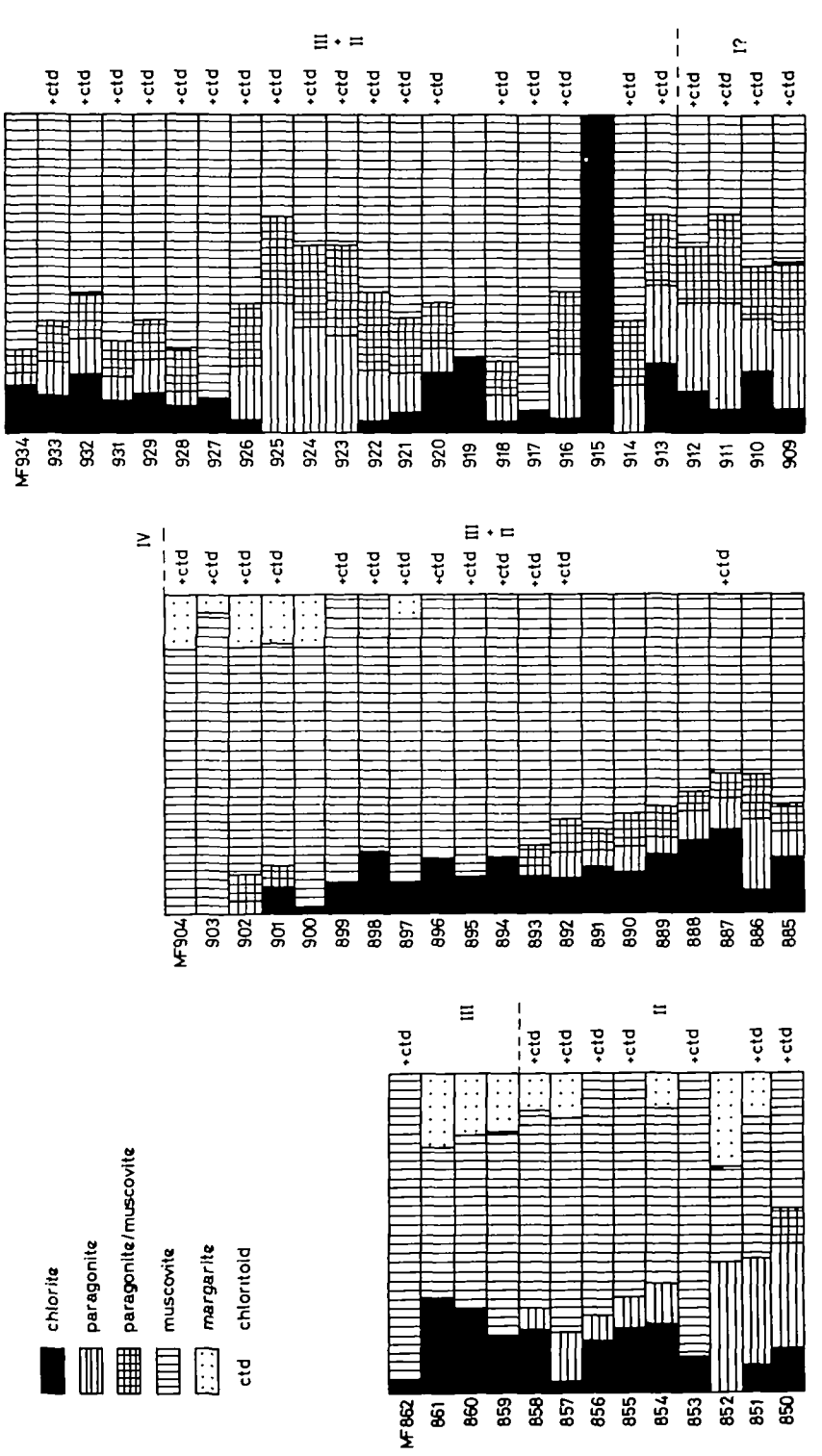

FIG. 7. Sheet silicate distribution (fraction $<2\ \mu$) in three stratigraphic sections from the Urseren Zone. I–IV designate lithostratigraphic units (members) within the Liassic of the Urseren Zone and may be correlated with corresponding units of the Glarus Alps (Fig. 5).

the measurement of the intensity-ratios of the first and the third basal reflexions (while this ratio is about 1 : 1 for paragonite, it is about 1 : 7 for margarite—Table 1). The last method works only if margarite clearly dominates over paragonite.

The mean *b* parameter of 10 samples was found to be 8·860 ± 0·005 Å, which is appreciably higher than the value of 8·837 ± 0·002 Å given by Chatterjee (1974*b*) for synthetic $2M_1$ margarite. This striking difference in *b* parameter is tentatively interpreted as being due to the solid solution of paragonite and/or ephesite in these margarites.

Chloritoid. Chloritoid is the only porphyroblastic mineral (long dimension 0·1–1·4 mm) in the Liassic formation of the Urseren Zone. It occurs as colourless, idioblastic crystals or rosettes with polysynthetic twinning and often with hour-glass structure. Only the triclinic modification is present (Halferdahl, 1961, table 17). Partial microprobe analyses of two grains (see Table 7 for coexisting minerals) yielded the following results:

	MF 81	MF 120
total Fe as FeO	24·2	23·3
MgO	2·9	3·7
MnO	0·44	0·31

TABLE 7

Modal and bulk rock composition of six epimetamorphic samples of the Urseren Zone

	MF 81	*MF 120*	*MF 852*	*MF 857*	*MF 886*	*MF 925*	*Average of 58 samples*
Muscovite	25	35–40	5–10	40	30	15	
Chlorite	—	—	—	<5	5	—	
Paragonite/muscovite	—	+?	—	—	5–10	10	
Paragonite	20	15–20	5–10	10	5–10	10–15	
Margarite	—	—	5	5–10	—	—	
Chloritoid	7	18	—	15	—	12	
Quartz	43	28	80	24	28	45	
Calcite	—	—	—	—	10	—	
Dolomite	—	—	—	—	14	—	
SiO_2	62·3	53·7	86·6	49·2	44·5	71·2	59·0
TiO_2	1·7	1·4	0·22	0·97	0·70	0·77	0·64
Al_2O_3	22·6	27·6	7·3$_5$	30·1$_5$	18·3	16·7$_5$	18·6
FeO*	3·6	5·3	1·2	6·8	4·8	3·8	5·5
MnO	0·07	0·06	<0·01	0·07	0·07	0·04	0·05
MgO	0·44	0·64	0·19	0·92	2·8	0·44	1·5
CaO	0·22	0·22	0·40	0·90	9·7	0·36	2·9
Na_2O	2·0	1·8	0·8	1·4	1·4	1·2	0·9
K_2O	2·6	3·7	0·9	4·2	3·4	1·8	3·6
P_2O_5	0·01	0·01	0·13	0·14	0·12	0·06	0·19
H_2O^+	3·0	4·9	0·95†	4·1†	2·8$_5$†	2·6†	3·5†
H_2O^-	0·21	0·44					
CO_2	—	—	0·06	0·05	10·7	0·04	2·8
C	0·54	0·71	0·21	1·1	0·64	0·33	0·53
S	n.d.	n.d.	n.d.	n.d.	n.d.	n.d.	0·18
Total	100·19	100·48	99·02	100·00	99·98	99·39	99·89

* Total Fe as FeO. †H_2O_{tot}.

Analyst M. Frey. The average chemical composition of 58 epimetamorphic phyllites and schists from Table 1 is shown for comparison. All values in wt. per cent.

The *other main phases* in the Liassic rocks of the Urseren Zone are quartz, ferroan calcite and ferroan dolomite. No feldspars were detected. The most frequent *accessory minerals* are pyrite, rutile, tourmaline and graphite (graphite d_{1A}—Landis, 1971).

Modal and bulk rock composition

The sheet silicate distribution of the $<2\ \mu$ fraction of three sections investigated is shown in Fig. 7. Muscovite is the dominant sheet silicate (30–95 per cent). Chlorite

TABLE 8

Mineral assemblages in 77 epimetamorphic phyllites and schists of the Urseren Zone

mu	*chl*	*pa/mu*	*pa*	*ma*	*ctd*	*cc*	*dol*	*Number of samples*
×	×	×	×		×			17
×	×				×			9
×	×		×		×			8
×		×	×		×			4
×	×	×	×		×	×		3
×			×		×			2
×	×	×	+?		×	×		1
×	×				×	×	×	1
×	×	+?	+?		×			1
×	×		×	×	×			3
×	×	×	+?	×	×			2
×				×	×			2
×	×			×	×	×		1
×	×			×	×			1
×	×			×				3
×				×		×	×	2
×	×	×	×	×		×		1
×			×	×				1
×	×	+?	×	×				1
×		×	+?	×		×	×	1
×	×			×		×	×	1
×	×	×	×			×		3
×	×	×	×			×	×	2
×	×	×	+?			×	×	1
×	×					×		2
×	×						×	1
×	×	×	+?					1
×	×		×					1
	×							1
76	65	36 + 2?	46 + 7?	19	55	19	9	77

Quartz and graphite are always additional phases.

(0–30 per cent, in one exceptional case 100 per cent) occurs in most samples. Paragonite (0–40 per cent) and/or mixed-layer paragonite/muscovite (0–30 per cent) are very common (Table 8), with the paragonite often predominating over the mixed-layer paragonite/muscovite (Fig. 7)—opposite to what was recorded from the Glarus Alps (Fig. 5). Margarite (0–30 per cent) is found in 19 out of 77 samples while chloritoid is present in 55 out of 77 samples.

Table 7 gives the mineralogical and chemical composition of 6 rocks, while Table 8 lists the mineral assemblages observed in 77 epimetamorphic samples of the Urseren Zone.

The epi- and mesometamorphic schists and phyllites of the Lukmanier area

116 epi- and mesometamorphic schists and phyllites from six sections of the Lower Liassic of the Lukmanier area were investigated. As Fox (1974, 1975) has studied the metapelites of the same formation in some detail, the present discussion is restricted to approximately 60 metasediments of marly composition. In addition, 10 samples from a Liassic section at Valle Cavalasca, about 15 km ENE of the Lukmanier Pass, were studied for comparison.

Mineralogy

Muscovite. X-ray investigation of the muscovites revealed exclusively 2M muscovites with negligible phengitic solid solution. This is corroborated by the microprobe data of Fox (1974) as well as that in Table 9.

Chlorite. X-ray data obtained from 7 marly samples indicate ripidolite compositions with wide range of Fe–Mg substitution. Microprobe data reproduced in Table 9 and additional ones by Fox (1974) are in agreement with this result.

Paragonite. Paragonite is a rare mineral in the marly rocks of the Lukmanier area although it was identified in a majority of the metapelites by Fox (1974) as well as by this author.

Margarite. Margarite was determined by X-ray methods described earlier. Once recognized, margarite could be distinguished in thin section from muscovite or paragonite through its lower birefringence and through its typical sheaf-like habit (Fig. 8). Margarite could also be found in fine, brownish intergrowths with

FIG. 8. Microphotograph of margarite in sample KAW 643 (Table 10). Plane polarized light. Length of picture corresponds to 0·7 mm.

TABLE 9

Chemical composition and structural formulae of some phases of the Lower Liassic of the Lukmanier Pass

	Muscovite MF 939	*Chlorite MF 939*	*Chloritoid MF 939*	*Ilmenite MF 939*	*Margarite KAW 643*	*Biotite KAW 643*	*Epidote MF 944*	*Calcite MF 944*	*Ankerite MF 944*
SiO_2	46·31	24·08	25·20	0·30	29·87	38·1	38·66	—	—
TiO_2	0·51	0·09	0·04	53·25	0·08	1·1	0·19	—	—
Al_2O_3	35·77	23·03	40·86	0·03	49·91	20·8	30·08	—	—
Fe_2O_3	—	—	—	—	—	$1·1_5$	4·52*	—	—
FeO	1·12†	25·76†	23·70†	46·08†	0·29†	16·7	—	3·62†	11·69†
MnO	0·00	0·06	0·18	0·67	0·00	0·04	0·06	0·23	0·24
MgO	0·66	13·74	3·06	0·07	0·08	10·0	0·09	1·50	13·44
CaO	0·02	—	—	0·00	12·63	0·45	23·83	50·74	29·38
Na_2O	1·27	—	—	—	0·96	0·16	—	—	—
K_2O	9·28	—	—	—	0·19	7·3	—	—	—
H_2O/CO_2						5·7		43·80‡	45·02‡
Total	94·94	86·76	93·04	100·40	94·01§	101·5	97·43	99·89	99·77
Number of ions on the basis of	22 (0)	28 (0)	12 (0)	6 (0)	22 (0)	22 (0)	$12\frac{1}{2}$ (0)	6 (0)	6 (0)
Si	6·15	5·14	2·05	$0·01_5$	4·03	5·58	2·99	—	—
Al	1·85	2·86	3·92	0·00	3·97	2·42	0·01	—	—
Al	3·75	2·94			3·97	1·14	2·73	—	—
Ti	0·04	0·02	0·00	1·99	0·01	0·12	0·01	—	—
Fe^{3+}	—	—	—	—	—	0·13	0·26	—	—
Fe^{2+}	0·12	4·60	1·61	1·93	0·03	2·05	—	0·10	0·32
Mn	0·00	0·01	0·01	0·03	0·00	0·01	0·04	0·01	0·01
Mg	0·13	4·37	0·37	0·01	0·02	2·18	0·01	$0·07_5$	0·65
Ca	0·00	—	—	0·00	1·82	0·07	1·97	1·82	1·02
Na	0·33	—	—	—	0·25	0·04	—	—	—
K	1·58	—	—	—	0·03	1·36	—	—	—

* Total Fe as Fe_2O_3. † Total Fe as FeO. ‡ CO_2 calculated on the basis of 2·00 C. § Includes 0·002 per cent Li_2O.
Analysts J. S. Fox and M. Frey.

groundmass paragonite. At first glance margarite may be mistaken for Mg-rich chlorite, but the higher relief and the positive elongation of margarite are characteristic. Microprobe analysis of one margarite is given in Table 9. Its optical data are: $n\gamma = 1{\cdot}648 \pm 0{\cdot}002$ and $2V = 45°$.

Biotite. Biotite porphyroblasts with a long dimension of up to 1 mm show the following pleochroism: $X.$ = light yellow, $Y = Z$ = brown. The wet chemical analysis of one biotite is presented in Table 9. Five biotites analysed by Fox (1974) from the Lower Liassic pelites are similar in composition.

Chloritoid. Chloritoid is mainly restricted to the basal pelitic part of the Lower Liassic formation but can occasionally be found in the northernmost calcareous schists of the Lukmanier Pass as well. In the southern part of this area, chloritoid occurs as armoured relics in garnet in both pelitic and marly rocks. It appears as pale bluish green to colourless laths of up to 1 mm in length. A microprobe analysis of one chloritoid is given in Table 9. According to the X-ray criteria of Halferdahl (1961) only the monoclinic modification is present in the 8 specimens examined thus far.

Kyanite and staurolite. Kyanite and staurolite are rare constituents in the calcareous schists of the southern part of the Lukmanier area. Detailed mineralogical data for these minerals in the Lower Liassic pelitic rocks can be found in Fox (1974).

Garnet. Garnet is a rare mineral in the calcareous schists of the northern part of the Lukmanier area but is widespread in equivalent rocks further south. The garnet porphyroblasts frequently contain inclusions of quartz, calcite and clinozoisite. Measurement of physical properties of 13 garnets gave $n = 1{\cdot}795$–$1{\cdot}809 \pm 0{\cdot}002$ and $a_0 = 11{\cdot}56$–$11{\cdot}62$ Å. From Winchell (1958, fig. 1) and assuming absence of Mn and Fe^{3+} in these garnets, the following compositional range may be estimated: 64–79 mole per cent almandine, 17–29 per cent grossularite and 3–12 per cent pyrope. This result compares favourably with microprobe data given by Fox (1974).

Clinozoisite. Clinozoisite, often with a core of pistacite, occurs as elongated prisms up to a few mm in length. A microprobe analysis of one clinozoisite is presented in Table 9.

Zoisite. Zoisite was detected in hand specimen only in the northern part of the Lukmanier area, where elongated porphyroblasts of several mm in length are common. In thin sections the porphyroblasts are strongly poikiloblastic with quartz and carbonate as main inclusions. The optical identification of zoisite was confirmed by X-ray analysis (see Seki, 1959). Zoisite from specimen MF 944, which seems to coexist with clinozoisite (4·52 per cent Fe_2O_3, Table 9) has a Fe_2O_3 content of 1·7 per cent. In another sample the Fe_2O_3 content of zoisite was found to be as low as 0·5 per cent.

Plagioclase. The composition of 9 plagioclases was determined by electron microprobe (Fox, 1974; Frey & Orville, 1974). In 9 additional samples they were estimated from $\Delta(131)$–$(1\bar{3}1)$ values using the curve of Bambauer *et al.* (1967). The compositions of all the plagioclases cluster in the range oligoclase–andesine.

The plagioclases in margarite-bearing samples, however, show the highest anorthite content.

Carbonate minerals. Ferroan calcite and ferroan dolomite have been identified by X-ray and by staining methods. The iron content seems to be dependent on the bulk composition. Table 9 lists analyses of calcite and ankerite from a relatively iron-rich specimen. A calcite from a sample poor in Fe was found to contain 0·6 per cent FeO and 2·0 per cent MgO whereas the coexisting dolomite contained 2·5 per cent FeO.

Opaques. Pyrrhotite, ilmenite, rutile and graphite (graphite d_1—Landis, 1971) are abundant accessory minerals while pyrite and secondary (?) hematite are rare. A microprobe analysis of an ilmenite is given in Table 9. Some pyrrhotites show a splitting of the (102) reflexion indicating that both a hexagonal and a monoclinic form are present.

Quartz is present as a major phase in all specimens studied. Tourmaline is

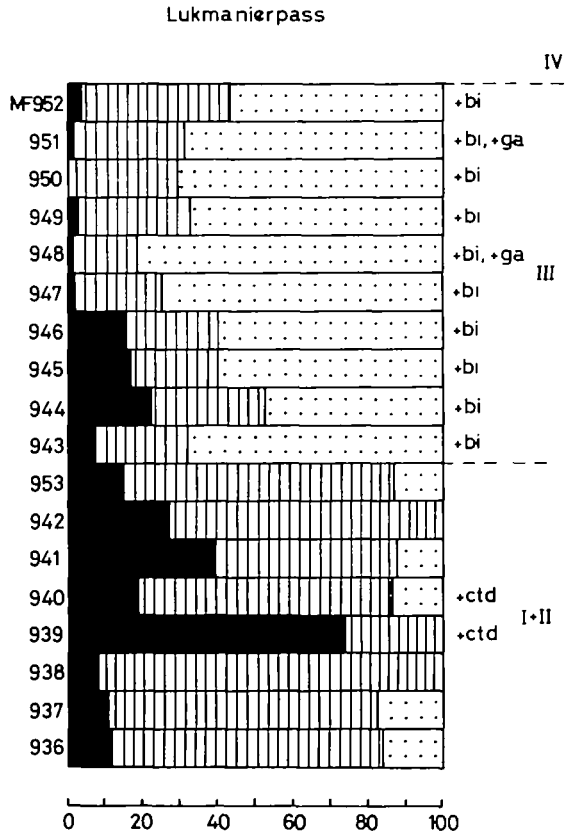

FIG. 9. Sheet silicate distribution (fraction <2 μ, biotite not taken into account) in a stratigraphic section at Lukmanier Pass. This section is located 1 km below the staurolite isograd as determined by Fox (1974, 1975). I–IV designate lithostratigraphic units (members) within the Liassic of the Lukmanier area and may be correlated with corresponding units of the Urseren Zone and the Glarus Alps (Frey, 1967, table 2). I = Lias-Basisquarzite, II = Basale Stgir-Serie, III = Untere Stgir-Serie, IV = Obere Stgir-Serie. Mineral symbols as in Fig. 7.

another accessory mineral besides the opaques. Staining with sodium cobaltnitrate showed that potassium feldspar was only present in two samples as a few, small isolated grains. Hornblende was found in a single sample from Val di Campo (kindly provided by Dr. J. Fox).

Modal and bulk rock composition

The sheet silicate distribution (excepting biotite) of the <2 μ fraction of the Lukmanier Pass section is shown in Fig. 9. There is a clear distinction between a pelitic lower and a calcareous upper part of the Lias. Muscovite is the predominant sheet silicate (25–90 per cent) in the lower part, but is less important (15–40 per cent) in the upper part. Chlorite (0–40 per cent, in one exceptional case 75 per

TABLE 10

Modal and bulk rock composition of six representative epi- and mesometamorphic samples from the Lukmanier area

	KAW 643	*MF 939*	*MF 944*	*MF 1601*	*MF 1611*	*MF 1621*	*Average of 18 samples*
Muscovite	30–35	5	15–20	15–20	15–20	15	
Chlorite	10–15	10–15	2	1	<1	1	
Paragonite	—	—	—	—	15–20	—	
Margarite	5–10	tr	10–15	<5	—	—	
Biotite	2	—	5	4	2	2	
Chloritoid	—	4	—	—	tr	—	
Staurolite	—	—	—	1	15	—	
Kyanite	—	—	—	1	2	—	
Garnet	—	—	—	7	3	5	
Clinozoisite	2	—	5*	1	<1	2	
Plagioclase	—	—	6	26	8	21	
Quartz	40	77	30	38	35	43	
Calcite	—	—	9½	3	—	4½	
Dolomite	5½	—	10½	—	—	4½	
Pyrrhotite	1½	—	2	tr	—	½	
Ilmenite	½	½	—	—	1½	1	
Rutile	—	—	tr	½	—	—	
SiO_2	68·7	87·6	52·5	50·6	51·9	55·6	54·4
TiO_2	0·62	0·43	0·19	0·71	1·3	0·75	0·80
Al_2O_3	12·9$_5$	4·6	14·6	21·3	29·8	17·0	16·8
FeO†	5·2	3·8	5·2	8·1	7·2$_5$	6·4	4·3
MnO	0·03	0·02	0·05	0·13	0·04	0·13	0·06
MgO	2·2	1·7	2·2	3·7	1·2	1·1	1·8
CaO	2·7	0·13	11·6	6·1	0·72	9·5	7·3
Na_2O	0·64	0·09	0·74	0·78	2·3	0·76	0·8
K_2O	3·2	0·42	2·7	3·3	2·6	2·3	4·6
P_2O_5	0·11	0·04	0·15	0·22	0·16	0·22	0·13
H_2O^+	1·4‡	1·5‡	1·4‡	2·8	3·4	1·7	1·3‡
H_2O^-				0·27	0·15	0·15	
CO_2	2·7	—	9·3	1·3	—	4·2	6·9
C	0·23	0·08	0·34	0·93	n.d.	0·57	0·40
S	n.d.	n.d.	n.d.	n.d.	n.d.	n.d.	0·28
Total	100·68	100·41	100·97	100·24	100·82	100·38	99·87

* Includes some zoisite. † Total Fe as FeO. ‡ H_2O_{tot}.

Analysts E. Regli and M. Frey. The average chemical composition of 18 epi- to mesometamorphic schists from Table 1 is shown for comparison. All values in wt. per cent.

TABLE 11

Mineral assemblages in 59 epi- and mesometamorphic schists of the Lukmanier area and 10 epimetamorphic phyllites and schists of Valle Cavalasca of marly composition

mu	*chl*	*pa*	*ma*	*bi*	*clz/zo*	gr	*plag*	*ctd*	*st*	*ky*	*cc*	*dol*	*Number of samples*
Valle Cavalasca, medium-grade epizone													
×	×	×	×								×	×	2
×	×	×	×								×		1
×	×	×	×		×		×				×	×	1
×	×	+?	×								×	×	1
×	×	+?	×								×		1
×	×	+?	×					×			×	×	1
×			×								×	×	1
×	×										×	×	1
×	×										×		1
10	9	4 + 3?	8		1		1	1			10	7	10
Lukmanier pass, higher-grade epizone													
×	×		×		×		×				×	×	5
×	×		×	×	×		×				×	×	3
×	×		×	×	×						×	×	2
×	×		×	×	×	×	×				×	×	2
	×			×	×	×					×		1
	×					×					×	×	1
×	×		×	×	×		×	(×)*			×	×	1
×							×	(×)*			×		1
×	×		×	×				×			×		1
×	×	×	×					(×)*			×		1
×	×	+?	×		×		×				×	×	1
×	×	+?	×		×		×				×		1
×	×	+?	×				×				×	×	1
×	×	+?	×				×				×		1
×		+?	×		×		×				×	×	1
×		+?	×				×				×	×	1
×	×	+?	×								×		1
×			×	×	×		×				×	×	1
×			×		×		×				×	×	1
×	×		×				×				×	×	1
×	×		×	×	×						×		1
×	×				×						×		1
Piorazone, lower-grade mesozone													
×	×			×	×	×	×				×	×	6
×	×		×	×	×	×	×				×	×	5
×	×		×	×	×	×	×				×		5
×			×	×	×	×	×				×	×	2
×			×	×	×	×	×				×		2
×				×	×	×	×				×	×	2
×				×	×		×				×	×	2
×	×		×	×	×	×	×	×	×		×		2
×	×			×	×	×	×	×	×		×		2
×	×			×	×	×	×		×		×		1
29	21		16	29	29	27	29	4	5		29	17	29

* Probably a relict.

Quartz and graphite are always additional phases.

cent) occurs in most samples but is rarer in biotite-bearing rocks of the upper part. Margarite is the major sheet silicate (45–80 per cent) in the upper part of the section studied.

Table 10 gives the mineralogical and chemical composition of 6 rocks. Samples MF 939 and 1611 are metapelitic rocks while the other four samples are marly metasediments.

Table 11 lists the mineral assemblages in 59 epi- and mesomatamorphic samples of marly bulk composition of the Lukmanier area as well as in 10 epimetamorphic samples from Valle Cavalasca. For a list of mineral assemblages in metapelitic rocks of this area the reader is referred to Fox (1974). An inspection of Table 11 reveals several interesting points. Essentially the same assemblages are found in the marly rocks of Valle Cavalasca as in those of the Urseren Zone. In contrast, paragonite still coexists with carbonate minerals at Valle Cavalasca whereas this assemblage was found with certainty in only one specimen at Lukmanier Pass and seems to be totally absent further to the south. A similar relationship holds true for chloritoid and carbonates.

At the Lukmanier Pass the most striking feature is the abundance of margarite. In the Piora Zone, approximately 6 km to the south, on the other hand, margarite seems to decrease both in its total abundance as well as in its average modal content. There, clinozoisite and plagioclase are widespread. Biotite and garnet make their appearance at Lukmanier Pass but are not yet common, while these minerals can be found in almost every specimen in the Piora Zone.

PROGRESSIVE METAMORPHISM

Mineral distribution

The mineral distribution along the metamorphic profile for the Lower Liassic black shale formation is summarized in Fig. 10. Since the outcrops studied were not continuous along the whole profile the mineral distribution shown is somewhat schematic. In particular, there is a gap in outcrops between the Urseren Zone and the Lukmanier Pass (Fig. 1). To fill out this gap additional information was taken from the southwestern end of the Gotthard Massif (Liszkay, 1965; Hansen, 1972; Frey & Orville, 1974) where the same formation can be studied in greater continuity.

Mineral reactions

Physico-chemical conditions of metamorphism may be more successfully derived from laboratory studies if specific metamorphic reactions are known from field data. In the following, several such mineral reactions will be discussed including the first appearance of pyrophyllite, paragonite, chloritoid, margarite and the high grade compatibility limits of paragonite and chloritoid in the presence of carbonates. The first appearance of plagioclase in this formation was discussed by Frey & Orville (1974) and therefore will not be dealt with here. The formation of biotite and garnet will not be discussed in this paper due to insufficient field data. Due to absence of continuous exposures the isograds were not mapped, although the rough positions were established. On the other hand, the mineral reactions

themselves were deduced from observed assemblages on both sides of these isograds.

Formation of pyrophyllite

The widespread occurrence of kaolinite and quartz in the unmetamorphosed sediments provides the most plausible starting material for the appearance of pyrophyllite in the Glarus Alps by virtue of the reaction

$$1 \text{ kaolinite} + 2 \text{ quartz} \rightarrow 1 \text{ pyrophyllite} + 1 \text{ } H_2O. \qquad (1)$$

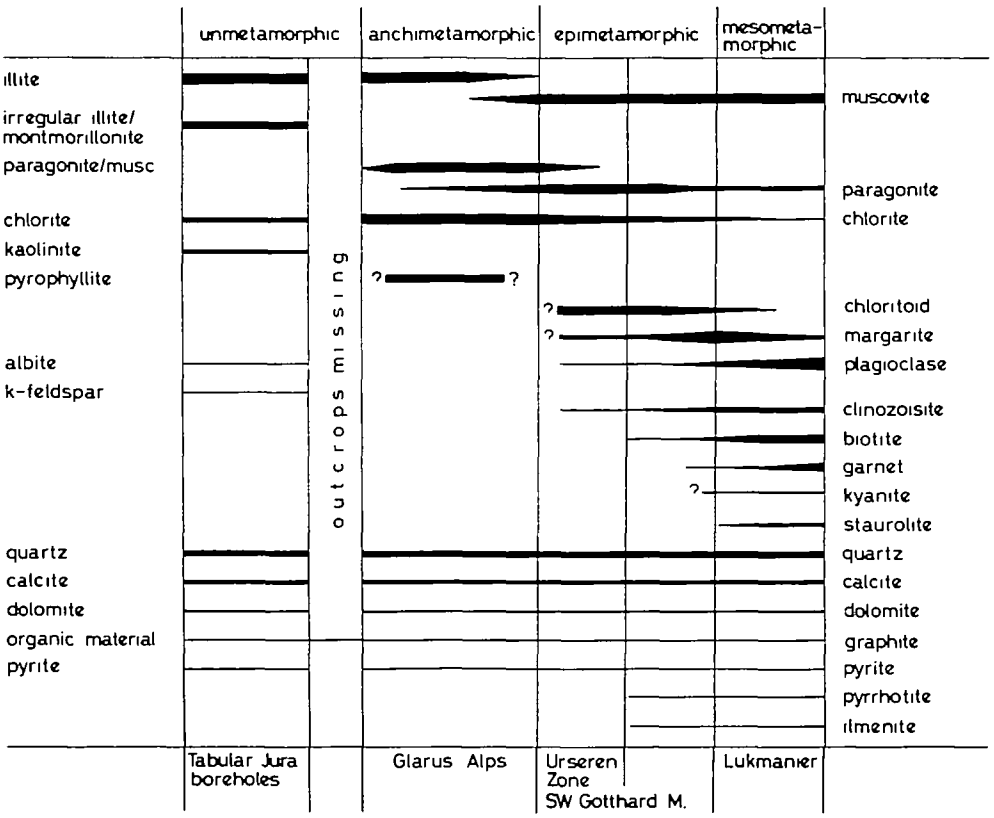

FIG. 10. Distribution of some important minerals of the Lower Liassic black shale formation. ? = distribution not clearly defined due to insufficient data.

An additional possibility is the formation of pyrophyllite at the expense of muscovite through the ionic reaction

$$2 \text{ muscovite} + 6 \text{ quartz} + 2 \text{ } H^+ \rightarrow 3 \text{ pyrophyllite} + 2 \text{ } K^+. \qquad (2)$$

Indeed, formation of rims of pyrophyllite around flakes of detrital muscovite has been observed in some of the rocks (cf. p. 106). However, the small quantity of detrital muscovite detected so far would indicate that reaction (2) can only be of minor significance.

Formation of paragonite

The observed sequence of appearance of sheet silicates from unmetamorphosed sediments to the anchizone is: irregular mixed-layer illite/montmorillonite → rectorite → mixed-layer paragonite/muscovite → discrete paragonite and muscovite. Furthermore, chemical data from rock B3 (Table 3) coupled with modal analysis suggests that the bulk of the sodium was held originally in the illite/montmorillonite structure. This would indicate that the illite/montmorillonite mixed-layer phase must have been the precursor of paragonite and part of the muscovite.

Formation of chloritoid

Nearly half of the anchizone Liassic rocks show the assemblage pyrophyllite–chlorite. By contrast, the higher grade assemblage in the epizone rocks are chloritoid + quartz with or without chlorite and without pyrophyllite. This clearly indicates that the phase chloritoid is ushered in by the reaction

$$\text{pyrophyllite} + \text{chlorite} \rightarrow \text{chloritoid} + \text{quartz} + H_2O, \qquad (3)$$

originally suggested by Zen (1960).

In the absence of chemical data on coexisting chloritoid and chlorite in rocks showing the *first* chloritoids, it is not yet possible to decide whether or not the chloritoid appears by reaction (3) in the pure Fe-system or by some complex reaction involving Fe–Mg crystalline solutions.

Formation of margarite

The anchizone rocks frequently contain the assemblage pyrophyllite–calcite, and more rarely pyrophyllite–dolomite. In the epizone rocks, these assemblages are excluded in favour of the assemblage margarite + quartz (with or without additional calcite and/or dolomite). These observations indicate the following mineral reactions:

$$\text{pyrophyllite} + \text{calcite} \rightarrow \text{margarite} + \text{quartz} + H_2O + CO_2 \qquad (4)$$

$$\text{pyrophyllite} + \text{dolomite} \rightarrow \text{margarite} + \text{chlorite} + \text{quartz} + H_2O + CO_2. \qquad (5)$$

There is some X-ray evidence that these margarites already contain significant amounts of paragonite in solid solution (see p. 112). This implies that some paragonite participates as a reactant in (4) and (5). Higher up in the metamorphic sequence, additional margarite is formed at the expense of the assemblages paragonite–calcite or chloritoid–calcite (see below).

Paragonite–carbonate relations

The assemblage paragonite–calcite, and less frequently, paragonite–dolomite is encountered in the Glarus Alps, the Urseren Zone, as well as in Valle Cavalasca (Fig. 1). At the Lukmanier Pass, paragonite–calcite is extremely rare. Further

south, both these assemblages apparently become incompatible while the phases plagioclase, margarite, and clinozoisite increase in abundance. The following mineral reactions might explain these observations:

$$\text{paragonite} + \text{calcite} + \text{quartz} \rightarrow \text{plagioclase} + \text{margarite} + H_2O + CO_2 \quad (6)$$

$$\text{paragonite} + \text{calcite} + \text{quartz} \rightarrow \text{albite} + \text{clinozoisite} + H_2O + CO_2 \quad (7)$$

$$\text{paragonite} + \text{dolomite} + \text{quartz} \rightarrow \text{plagioclase} + \text{margarite} + \text{chlorite} + H_2O + CO_2 \quad (8)$$

$$\text{paragonite} + \text{dolomite} + \text{quartz} + H_2O \rightarrow \text{albite} + \text{chlorite} + \text{calcite} + CO_2. \quad (9)$$

For the association of plagioclase with margarite instead of albite, see Frey & Orville (1974).

The disappearance of chloritoid in marly rocks

The assemblage chloritoid–calcite, with grains bearing clean, unreacted boundaries is common (Table 8) in the epimetamorphic Urseren Zone. At the Lukmanier Pass, however, this assemblage was only found once. Further upgrade, it is pseudomorphically replaced by chlorite and white mica; or else, chloritoid remnants are observed surrounded by zoisite porphyroblasts. Possible reaction relations are:

$$\text{chloritoid} + \text{calcite} + \text{quartz} + H_2O \rightarrow \text{chlorite} + \text{margarite} + CO_2 \quad (10)$$

$$\text{chloritoid} + \text{calcite} + \text{quartz} + H_2O \rightarrow \text{chlorite} + \text{zoisite} + CO_2. \quad (11)$$

It is worth noting that stable chloritoid–calcite assemblages have also been reported from other Alpine localities (cf. Niggli, 1965; Chatterjee, 1971).

Distribution of margarite in the Lukmanier area

Margarite is much more frequent and quantitatively important at the Lukmanier Pass than in the Urseren Zone. This might be the consequence of tie line changes resulting from reactions (6), (8) and (10), although the effect of local variation in bulk compositions can not be ruled out. Further upgrade, towards the Piora Zone (Fig. 1), margarite becomes less abundant; at the same time the plagioclase content seems to increase from 8 to 25 per cent. In the absence of data on the composition of the coexisting phases, these observations are interpreted to indicate that margarite is used up through a continuous reaction to produce plagioclase along with other phases.

PHASE RELATIONS

The mineral assemblages dealt with in the foregoing sections can be represented by the multicomponent system SiO_2–Al_2O_3–Fe_2O_3–FeO–MgO–MnO–CaO–Na_2O–K_2O–H_2O–CO_2. Fortunately, not all these components need to be regarded as *determining components* because:

(i) Quartz is ubiquitous as a pure phase, justifying the treatment of SiO_2 as an *excess component*.

(ii) Organic material or graphite is invariably associated with H_2O-bearing phases in these rocks. This implies that fluid species belonging to the system C–O–H, which include H_2O, CO_2, CH_4, H_2, O_2, CO etc., were present during metamorphism. In handling the mineral equilibria, all other gas species save H_2O and CO_2 can be treated as inert dilutants of the equilibrium fluid.

(iii) Muscovite, with negligible phengitic content, is present in all the assemblages. For this reason, the phase relations can be projected from $KAl_3Si_3O_{10}(OH)_2$.

These considerations lead to the recognition of 7 determining components (Al_2O_3, Fe_2O_3, FeO, MgO, MnO, CaO, Na_2O) and 4 excess components (KAl_3O_5, SiO_2, H_2O and CO_2). For the moment, the phase relations will be treated in terms of two *quaternary model subsystems*, with 4 excess components in each case. These model subsystems are:

(1) Na_2O–CaO–Al_2O_3–MgO (plus excess KAl_3O_5–SiO_2–H_2O–CO_2), and
(2) Na_2O–CaO–Al_2O_3–FeO (plus excess KAl_3O_5–SiO_2–H_2O–CO_2).

In discussing the phase equilibria, another simplification will be introduced at this point, namely that the solid solubilities of the various phases will be ignored, *i.e.*, all the phases will be handled as if they were pure end-members.

Phase relations in the two model systems can be considered with respect to the following variables: P_{total}, P_{fluid}, T, and the composition of the equilibrium fluid. As all condensed phases are considered to be pure solids with unit activities, no other compositional variables are involved. The phase relations will be indicated in isobaric ($P_{total} = P_{fluid}$) T–X_{CO_2} sections. Note that due to presence of gas species other than H_2O and CO_2, the sum of the partial pressures of H_2O and CO_2 will in general be less than P_{fluid}.

This treatment differs from that of Chatterjee (1971) in that muscovite is present in all assemblages (plus quartz) and FeO and MgO are treated as separate (but insoluble for the present) components. Consequently, both components Na_2O and KAl_3O_5 can be shown with one tetrahedron and Fig. 11 in this paper may be compared with Plate 1 of Chatterjee (1971). It should be noted that paragonite and dolomite, which form a compatible assemblage as shown here, were considered to be incompatible by Chatterjee (1971).

The subsystem Na_2O–CaO–Al_2O_3–MgO–(KAl_3O_5–SiO_2–H_2O–CO_2)

The phases pyrophyllite, margarite, clinozoisite–zoisite, calcite, dolomite, chlorite, paragonite and plagioclase belong to this MgO-subsystem and were observed in samples from the anchizone to the epizone. Plagioclase was assumed to be albite; consideration of anorthite as an additional end-member phase in this system leads to the somewhat more complex phase relations discussed elsewhere (Frey & Orville, 1974).

Due to the highly degenerate nature of the system only 17 isobaric univariant reactions need be considered (Table 12). As none of these reactions has been experimentally investigated, the phase relations presented in Fig. 11 were derived from some of the observed mineral assemblages and mineral reactions.

The phase equilibria in the limiting subsystem Na_2O–CaO–Al_2O_3–(KAl_3O_5–SiO_2–H_2O–CO_2), which includes the phases Py, Ma, Zo, Cc, Pa and Ab (plus excess muscovite, quartz and vapour), were developed earlier for similar rocks by Frey & Orville (1974, fig. 4). These phase relations, which constitute the seven isobaric invariant lines emanating from the isobaric invariant points I_2 and I_4 in Fig. 11, have been adopted without modification. The presence of a fourth

TABLE 12

Isobaric univariant reactions in the two modal subsystems Na_2O–CaO–Al_2O_3–MgO or FeO–(KAl_3O_5–SiO_2–H_2O–CO_2), with the 8 phases Py, Ma, Zo, Cc, Dol or Ctd, Chl, Pa, and Ab with muscovite, quartz and vapour present in excess

Linear degenerate reactions (on edges of compositional tetrahedron)		
1.	(—)	1 Pa + 4 Qz = 1 Py + 1 Ab
2.	(—)	5 Py + 2 Zo = 4 Ma + 18 Qz + 2 H_2O
3.	(—)	2 Py + 1 Cc = 1 Ma + 6 Qz + 1 H_2O + 1 CO_2
4.	(—)	3 Py + 4 Cc = 2 Zo + 6 Qz + 2 H_2O + 4 CO_2
5.	(—)	3 Ma + 5 Cc + 6 Qz = 4 Zo + 1 H_2O + 5 CO_2
18.	(FeO)	6 Py + 2 Chl = 9 Ctd + 20 Qz + 5 H_2O
Planar degenerate reactions (with crossing tie-lines on triangular faces of compositional tetrahedron)		
6.	(—)	3 Pa + 4 Cc + 6 Qz = 2 Zo + 3 Ab + 2 H_2O + 4 CO_2
7.	(—)	2 Pa + 1 Cc + 2 Qz = 1 Ma + 2 Ab + 1 H_2O + 1 CO_2
8.	(—)	5 Pa + 2 Zo + 2 Qz = 5 Ab + 4 Ma + 2 H_2O
9.	(MgO)	21 Py + 9 Dol = 9 Ma + 2 Chl + 61 Qz + 4 H_2O + 18 CO_2
10.	(MgO)	39 Py + 36 Dol + 2 H_2O = 18 Zo + 8 Chl + 82 Qz + 72 CO_2
11.	(MgO)	3 Py + 9 Dol + 5 H_2O = 2 Chl + 9 Cc + 7 Qz + 9 CO_2
12.	(MgO)	39 Ma + 45 Dol + 73 Qz + 22 H_2O = 42 Zo + 10 Chl + 90 CO_2
13.	(MgO)	3 Ma + 18 Dol + 4 Qz + 13 H_2O = 4 Chl + 21 Cc + 15 CO_2
14.	(MgO)	6 Chl + 39 Cc + 3 Qz + 15 CO_2 = 6 Zo + 27 Dol + 21 H_2O
19.	(FeO)	6 Pa + 2 Chl + 4 Qz = 6 Ab + 9 Ctd + 5 H_2O
20.	(FeO)	27 Ctd + 24 Cc + 24 Qz + 3 H_2O = 6 Chl + 12 Zo + 24 CO_2
21.	(FeO)	10 Chl + 24 Ma + 8 Qz = 45 Ctd + 12 Zo + 13 H_2O
22.	(FeO)	9 Ctd + 3 Cc + 2 Qz + 2 H_2O = 3 Ma + 2 Chl + 3 CO_2
Volume reactions (piercing of internal planes within tetrahedron)		
15.	(MgO)	21 Pa + 9 Dol + 23 Qz = 21 Ab + 9 Ma + 2 Chl + 4 H_2O + 18 CO_2
16.	(MgO)	39 Pa + 36 Dol + 74 Qz + 2 H_2O = 39 Ab + 18 Zo + 8 Chl + 72 CO_2
17.	(MgO)	3 Pa + 9 Dol + 5 Qz + 5 H_2O = 3 Ab + 2 Chl + 9 Cc + 9 CO_2

(—) involves no FeO or MgO.

determining component, MgO, and the two additional phases Chl and Dol generates nine additional mineral equilibria, seven of which are shown in Fig. 11. This T–X_{CO_2} grid includes 17 isobaric divariant fields. For each of these divariant fields, one compatibility tetrahedron has been constructed.

A comparison of Fig. 11 with observed natural assemblages (Tables 6, 8 and 11) brings up the following interesting points:

(i) The grid is divided into four sectors with respect to the occurrences of zoisite and margarite through the isobaric invariant point I_2. At relatively low temperature and relatively high X_{CO_2} neither zoisite nor margarite is stable. At relatively low

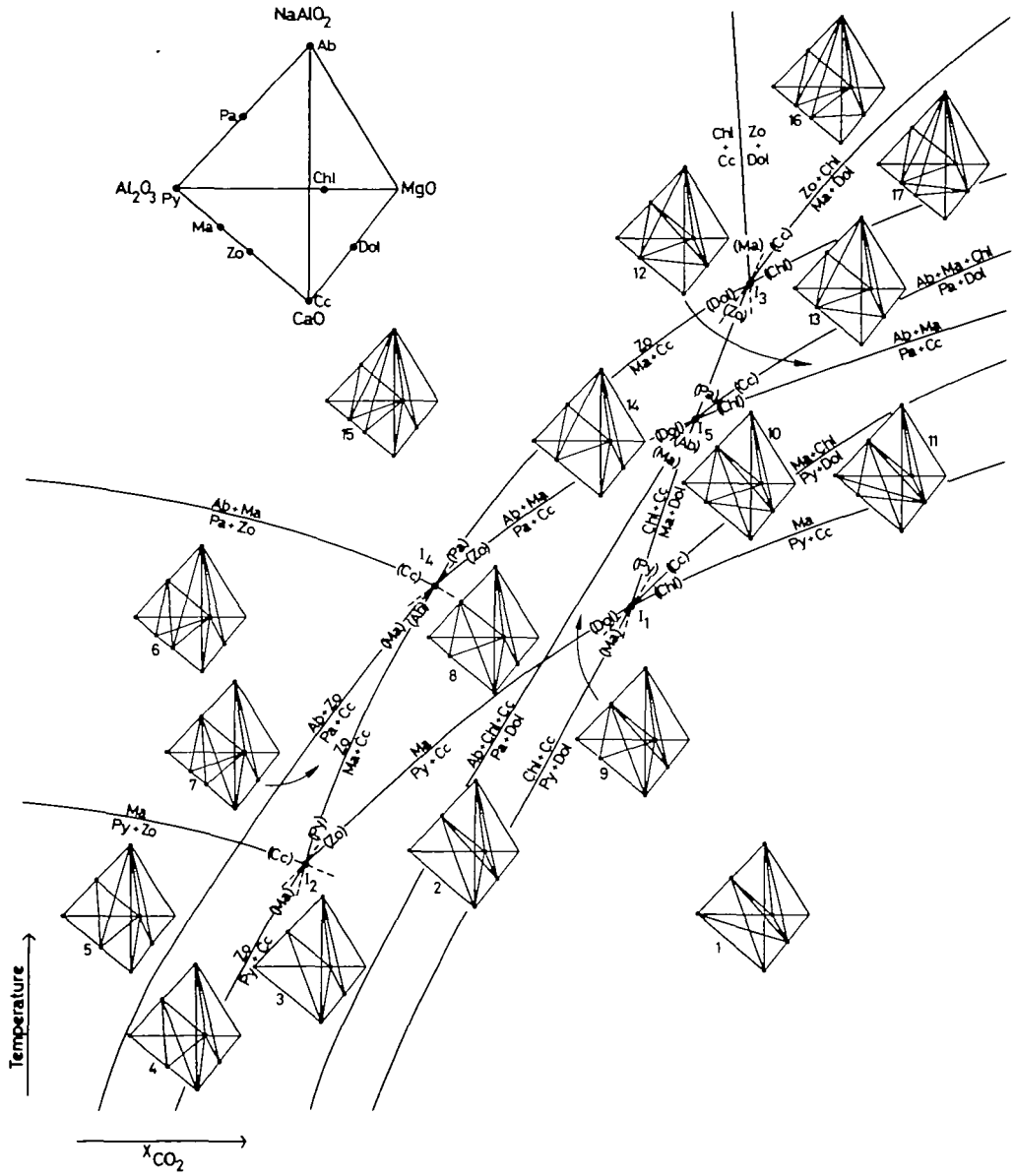

FIG. 11. Schematic isobaric temperature–fluid composition diagram for the modal subsystem Na_2O–CaO–Al_2O_3–MgO–(KAl_3O_5–SiO_2–H_2O–CO_2) with the 8 phases Py, Ma, Zo, Cc, Dol, Chl, Pa, and Ab with muscovite, quartz and vapour present in excess.

temperature and X_{CO_2}, however, zoisite alone is stable (to the left of the curve Py + Cc = Zo and below the curve Py + Zo = Ma).

At intermediate temperatures and at relatively high X_{CO_2} margarite alone is stable (above the curve Py + Cc = Ma and below or to the right of the curve Ma + Cc = Zo). Finally, zoisite and margarite together are stable over a wide field of temperature and X_{CO_2} (above the curve Py + Zo = Ma and above or to the left of the curve Ma + Cc = Zo). Note that as far as absolute values of X_{CO_2} are

concerned, the grid shown in Fig. 11 has to be placed within the stability field of zoisite, which is restricted to water-rich fluid compositions ($X_{CO_2} \leqslant 0{\cdot}1$ at a total pressure $\leqslant 5$ kb, Nitsch & Storre, 1972; Johannes & Orville, 1972; Hewitt, 1973).

(ii) The petrogenetic significance of the various isobaric divariant assemblages is different. For instance, the assemblage Py–Pa–Ma–Chl is common, occurring in the divariant fields 6–10 and 12–17, and therefore cannot be used to limit T and X_{CO_2}. In contrast, the assemblage Py–Pa–Cc–Chl, which is quite common in the Glarus Alps (Table 6), is restricted to isobaric divariant fields 2 and 3 only. Even more critical is the assemblage Ma–Ab(Plag)–Cc–Chl, found only once at Lukmanier Pass (Table 11), which is diagnostic only of the isobaric divariant field 14. If constraints could be set on temperature and fluid composition, therefore,

TABLE 13

Apparent variance of observed assemblages in the isobaric T–X_{CO_2} diagrams of Figs. 11/12

Variance	*−1*	*0*	*1*	*2*	*⩾3*
Glarus Alps anchimetamorphic	0/0	0/0	4/0	19/14	85/95
Urseren zone, lower-grade epizone	0/0	0/0	2/1	5/10	71/66
Valle Cavalasca and Lukmanier Pass higher-grade epizone	7/0	0/1	8/10	4/7	7/9

The variance was determined relative to the components of the model systems.

even these divariant assemblages would be diagnostic with regard to the metamorphic conditions.

(iii) Observed isobaric 'divariant' assemblages (for a discussion of the true variance see below) from the different areas of investigation plot in the following fields: Glarus Alps: 2, 3, 9; Urseren Zone: 2, 8, 9, 10, 11; Valle Cavalasca and Lukmanier Pass: 8, 9, 12, 13, 14. This pattern is consistent with an increase in temperature southwards from the Glarus Alps to the Lukmanier Pass, whereas there is only a weak indication that X_{CO_2} was generally increasing in the same direction.

(iv) The apparent variance of observed assemblages (see below) generally decreases with increasing metamorphic grade (Table 13). The occurrence of isobaric univariant assemblages on a T–X_{CO_2} diagram may be interpreted to mean that the system buffered its own fluid composition. However, the *true variance* of the observed natural assemblages will be much higher than indicated in Table 13 because at least two determining components (*e.g.* FeO, MnO) have been disregarded in the model MgO-system. Moreover, the total pressure might not have been constant along the metamorphic profile.

The subsystem Na_2O–CaO–Al_2O_3–FeO–(KAl_3O_5–SiO_2–H_2O–CO_2)

Eight phases belonging to this quaternary FeO-model system were observed from the anchizone to the epizone: pyrophyllite, margarite, clinozoisite-zoisite, calcite, chlorite, chloritoid, paragonite and plagioclase. Once again, the phase

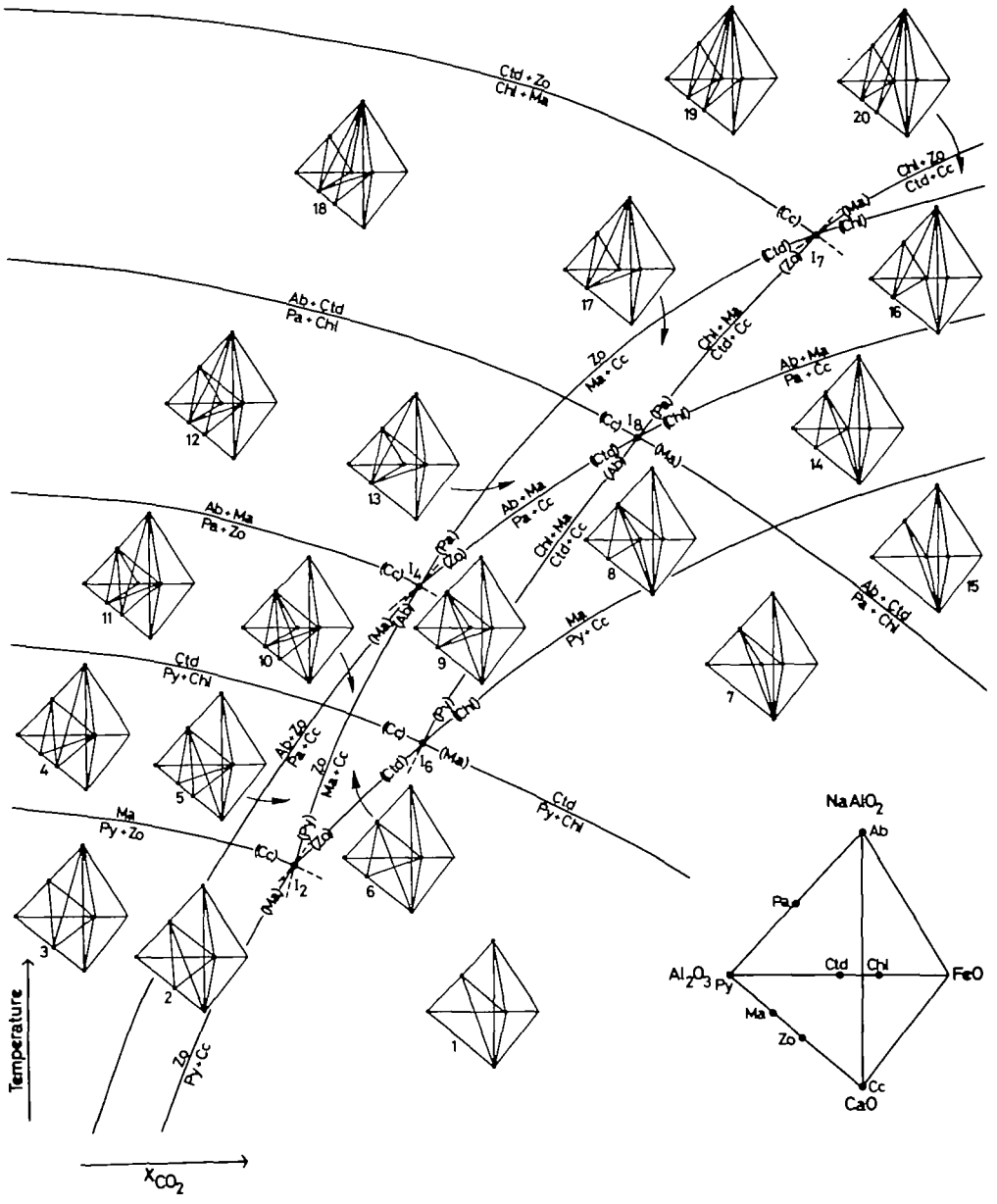

FIG. 12. Schematic isobaric temperature–fluid composition diagram for the subsystem Na_2O–CaO–Al_2O_3–FeO–($KAlO_5$–SiO_2–H_2O–CO_2), with the 8 phases Py, Ma, Zo, Cc, Chl, Ctd, Pa, and Ab with muscovite, quartz and vapour present in excess.

relations have been derived solely on the basis of the end-member composition (see p. 124). As this subsystem is highly degenerate, only 13 isobaric univariant reactions exist (Table 12). Of these, eight were already encountered in the subsystem treated earlier.

The phase relations can again be demonstrated on an isobaric ($P_{fluid} = P_{total}$) T–X_{CO_2} diagram. Note that the mass balance relations for the individual reactions

(Table 12) do not involve participation of O_2. As such, oxygen fugacity need not be considered as an additional intensive variable.

As with Fig. 11, a number of interesting points can be made by comparing Fig. 12 with the observed natural assemblages:

(i) As in Fig. 11 the grid is divided into four sectors around the isobaric invariant point I_2 with regard to the occurrences of zoisite and margarite.

(ii) The assemblage Ctd–Cc is stabilized at a relatively high X_{CO_2} although the absolute value of X_{CO_2} must still be low. This is so because the Ctd–Cc compatibility field lies within the stability limit of zoisite, which itself is indicative of low X_{CO_2}.

(iii) Observed isobaric 'divariant' assemblages plot in the following fields: Glarus Alps: 1; Urseren Zone: 7–13; Valle Cavalasca and Lukmanier Pass: 6, 9, 13, 17. Once again, this pattern is consistent with temperature increasing southwards but nothing can be said with respect to a possible change in X_{CO_2}.

(iv) As before, the apparent variance of observed assemblages generally decreases with increasing metamorphic grade (Table 13). The common occurrence of isobaric low-variance assemblages in the higher-grade epizone may indicate some internal buffering of the fluid phase or conditions favouring increasing disequilibrium. However, since the true variance of the observed assemblages may be much higher due to neglected components, this statement may not hold true.

It is clear that the natural reactions involved, at least, Fe–Mg crystalline solutions and it is necessary to combine the grids shown in Figs. 11 and 12. However, without detailed compositional data many ambiguities exist in the relative locations of the equilibria. Work is in progress to determine the possible effects of such crystalline solutions on the reactions observed.

PHYSICAL CONDITIONS DURING METAMORPHISM

If chemical equilibrium can be assumed, the physical conditions during metamorphism can be deduced from laboratory-calibrated mineral equilibria. This will be attempted for the rocks of the anchizone (Glarus Alps) and epi–mesozone (Lukmanier area).

Physical conditions for the anchimetamorphic Glarus Alps

Homogenization *temperatures* of fluid inclusions in fissure minerals can only be used to obtain minimum temperatures of metamorphism. This is because microthermometry measurements are often done on secondary inclusions; moreover, fissure minerals are known to form after the peak of metamorphism, although possibly not much later (see *e.g.* Poty & Stalder, 1970, p. 150). Homogenization temperatures of the order of 220 °C were obtained by Stalder & Touray (1970) on fissure quartz from a large number of localities in the Helvetic Nappes west of Lake Lucerne (Fig. 1). Most of these occurrences are in much the same tectonic and metamorphic setting as is the Liassic black shale formation of the northern and central Glarus Alps (Spitzmeilen and Klausenpass areas, Fig. 1),

so that temperatures slightly in excess of 220 °C seem to be indicated for the northern part of the Liassic sequence in the Glarus Alps.

No *pressure* indication can be obtained from the mineral compatibilities of the Liassic metasediments. However, laumontite is known from the Taveyanne graywackes of the northern Glarus Alps (Frey & Niggli, 1971, p. 232) while lawsonite has not been reported thus far. From the virtually pressure-independent

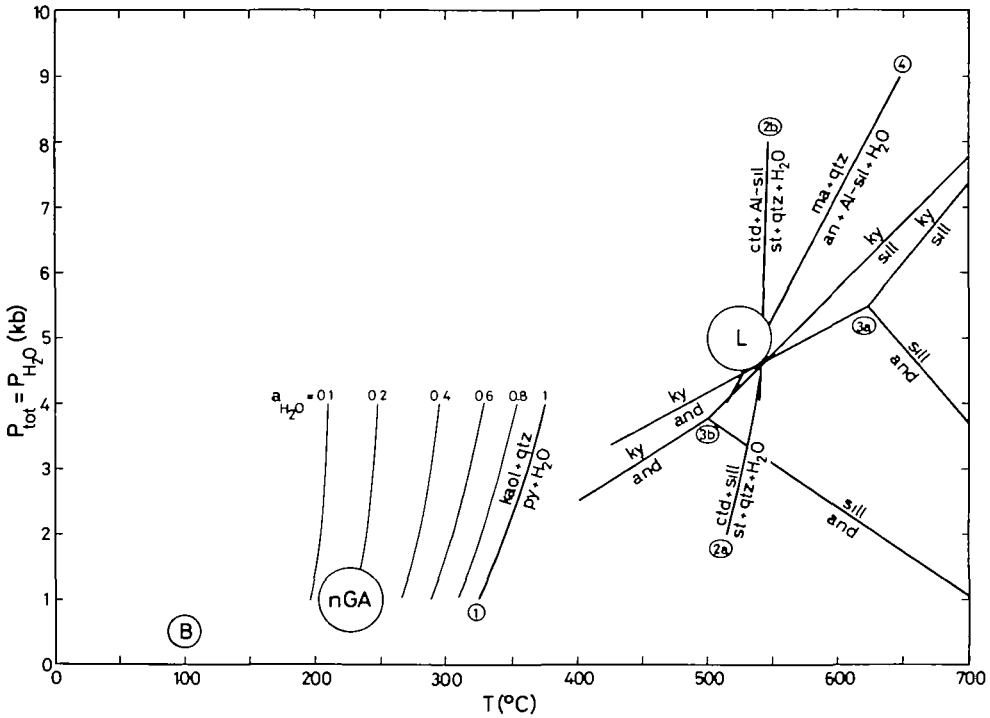

FIG. 13. Some calibrated reactions relevant to this study. The sources of data are as follows:
1 Thompson (1970*a*) for a_{H_2O} 1. Calculated equilibria for different water activities are shown.
2a Richardson (1968).
2b Hoschek (1967, 1969).
3a Richardson *et al.* (1969).
3b Holdaway (1971).
4 Storre & Nitsch (1974).
Estimated *P–T* conditions are shown for the boreholes under the Molasse Basin (B), the northern Glarus Alps (nGA), and the Lukmanier area (L).

transition curve lawsonite → laumontite (Nitsch, 1968; Thompson, 1970*b*; Liou, 1971), therefore, it would seem that a maximum total pressure of 3 kb was attained here. From a stratigraphic–tectonic viewpoint, Trümpy (in Hsu, 1969, p. 147) suggested that the total Glarus overthrust may have been 5–6 km thick, giving a lithostatic pressure of about 2 kb. This pressure estimate would be slightly reduced by the fact that the Spitzmeilen area lies approximately 1–2 km above the Glarus overthrust (see *e.g.* Trümpy, 1969, plate I).

Some evidence regarding the *composition of the metamorphic fluids* may be derived from the data of French (1966) and Eugster & Skippen (1967). According

to them, the composition of the fluids is graphite-bearing rocks at low temperatures and pressures is strongly dependent on the oxygen fugacity. From an investigation of isotopic compositions of carbonaceous materials in these rocks, Hoefs & Frey (1976) concluded that the oxygen fugacity was near to that of the QFM buffer. From Eugster & Skippen (1967, fig. 3), at 300 °C and 2 kb P_{total}, the fluid in equilibrium with graphitic material on the QFM buffer will be predominantly methane. Fluid inclusion studies on diagenetic and anchimetamorphic rocks of the Helvetic Zone (Stalder & Touray, 1970; Touray *et al.*, 1970; Mullis, 1975) also indicate fluids very rich in methane, but poor in H_2O and CO_2. This conclusion is further corroborated by the widespread occurrence of pyrophyllite, rather than kaolinite + quartz in these anchizone rocks. According to Thompson (1970*a*), the equilibrium temperature of the reaction Kaol + Qtz → Py + H_2O is approximately 330–340 °C at a P_{H_2O} of 2 kb. Thermodynamic calculations demonstrate that at an estimated temperature around 220 °C and at a P_{total} of 1–2 kb, pyrophyllite is stabilized at the expense of kaolinite + quartz only if a_{H_2O} is of the order of 0·1 to 0·2 (Fig. 13).

Physical conditions for the epi- and mesometamorphic rocks of the Lukmanier area

The metamorphic conditions for the Lukmanier area have already been discussed in some detail by Frey (1969*a*) and by Fox (1974, 1975). For the Lukmanier Pass, they estimated a *temperature* around 500 °C, and for the Piora Zone, approximately 550 °C.

In the following, an attempt will be made to apply yet another method to the estimation of temperature. Estimates from muscovite–paragonite solvus calibrations give anomalously high temperatures. However, by using the correlation between muscovite–paragonite and calcite–dolomite as proposed by Rosenfeld (1969, pp. 343–4) temperatures of 500 °C for the mesometamorphic rocks of the Piora Zone were obtained. This value seems to be rather low.

Kyanite is the widespread Al_2SiO_5 phase in the Lukmanier area. Recently, Rosenfeld in Adams *et al.* (1975) has described late sillimanite needles growing at the expense of kyanite in one sample from the Piora Zone. Assuming that the major episode of metamorphism did take place within the stability field of kyanite, a minimum confining *pressure* of 4–5 kb at a temperature of 500–550 °C is indicated by the experimental data of Newton (1966), Richardson *et al.* (1969) and Holdaway (1971).

From the indifferent crossing of the equilibrium curves pertaining to the upper compatibility limit of margarite + quartz and the lower compatibility limit of staurolite + quartz Fox (1975) suggested a minimum P_{total} ($=P_{H_2O}$) of 5·5 kb.

Investigation of piezobirefringent halos of quartz inclusions in garnet from the Piora Zone rocks led Adams *et al.* (1975) to conclude that a confining pressure of 4·3 kb obtained during the metamorphism of these rocks. Using a temperature estimate of 550 °C, rather than 515 °C, their data can be used to yield a pressure of 5·0 ± 0·3 kb.

Some information on the *composition of the metamorphic fluid* may be extracted

from the mineralogical data given earlier. Thus, by knowing the temperature of metamorphism and the composition of ilmenite solid solution (Fox, 1974, and Table 9 here), a minimum f_{O_2} value of 10^{-26} to 10^{-28} bar is obtained according to experimental data of Buddington & Lindsley (1964, fig. 5). Extensive occurrence of clinozoisite and/or zoisite would indicate the presence of a water-rich fluid. According to experimental data by Nitsch & Storre (1972), Johannes & Orville (1972) and Hewitt (1973), an X_{CO_2} value $\leqslant 0{\cdot}08$ can be assessed for the present area.

Geothermal and thermal gradients

Directly measured and calculated values of geothermal gradients for three localities along the metamorphic profile are listed in Table 14. The calculated

TABLE 14

Local geothermal gradients for different areas along the metamorphic profile studied derived from P–T conditions estimated from mineral stabilities as well as other petrographic methods and tectonic reasonings

Area	*T °C*	*P kb*	*Rock density in gr/cm³*	*Overburden in km*	*Local geothermal gradient °C/km*
Boreholes below the Molasse Basin	100*	—	—	2–2·3	43–50
Northern Glarus Alps	200–250	—	—	4	50–62
Lukmanier area	500–550	5	2·85†	17·9	28–31

* Measured borehole temperature, Büchi, pers. comm. 1972.
† Value taken from Frey (1969*a*, fig. 33).

geothermal gradient (about 28–31 °C/km) for the Lukmanier area fits into the range of 20–40 °C/km given by Clark & Jäger (1969, p. 1156) for the Central Alps (Lepontine region). The value for the northern Glarus Alps gives higher gradients (50–62 °C/km) due to lower metamorphic pressures. This latter region presumably records a 20–25 my event (Hunziker, work in progress) whereas the Lukmanier region records the same event (Köppel & Grünenfelder, 1975) or a 35–38 my event (Hunziker, 1969; Jäger, 1973). It should be noted that present day measurements in boreholes below the Molasse Basin in the vicinity of Lindau imply local gradients of 43–50 °C/km. However, possible interpretations and consequences of these results have to be postponed, until the following points are clarified: (i) Did the metamorphism of the Helvetic and the Pennine Zone take place during the same orogenic phase? (ii) To what extent were the Glarus Alps affected by postmetamorphic tectonic transport?

As far as the thermal gradient along the metamorphic profile is concerned, an average gradient of 30 °C/km is obtained (Fig. 13). This gradient would imply that the metamorphic process described here belongs to the medium-pressure or kyanite–sillimanite type of Miyashiro (1961).

ACKNOWLEDGMENTS

I am indebted to Prof. E. Niggli for his support throughout this study and to Prof. T. Hügi who kindly made his laboratory available for chemical analyses. I would also like to thank Mrs. E. Regli for her wet chemical analyses, Dr. F. Hofman for his sulphur and carbon determinations and T. Küpfer and E. Frank for their laboratory assistance.

Dr. U. P. Büchi, Swiss Petrol Company, and the Gewerkschaft Elwerath, Erdölwerke Hannover kindly supplied specimens from the boreholes below the Molasse Basin.

I would like to acknowledge stimulating discussions had with N. D. Chatterjee, J. S. Fox, C. V. Guidotti, J. C. Hunziker, E. Jäger, E. Niggli, P. M. Orville, T. Peters, J. Rosenfeld, H. A. Stalder and P. Thompson, and the help of N. D. Chatterjee, J. S. Fox, C. V. Guidotti, A. B. Thompson and E-an Zen in the preparation of the manuscript. However, the responsibility for anything presented here is entirely mine.

This work was supported by grants from the Schweizerischer Nationalfonds (No. 5358.2 and 2.838.73) and the Forschungskommission der Universität Bern.

REFERENCES

ADAMS, H. G., COHEN, L. H., & ROSENFELD, J. L., 1975. Solid inclusion piezothermometry: II. Geometric basis, calibration for the association quartz–garnet, and application to some pelitic schists. *Am. Miner.* **60**, 584–98.

BAMBAUER, H. U., CORLETT, M., EBERHARD, E., & VISWANATHAN, K., 1967. Diagrams for the determination of plagioclases using X-ray powder methods. *Schweiz. Miner. petrogr. Mitt.* **47**, 333–49.

BAUMER, A., FREY, J. D., JUNG, W., & UHR, A., 1961. Die Sedimentbedeckung des Gotthard-Massivs zwischen oberem Bleniotal und Lugnez. *Eclogae geol. Helv.* **54**, 478–91.

BENCE, A. F., & ALBEE, A. L., 1968. Empirical correction factors for the electron micro-analysis of silicates and oxides. *J. Geol.* **76**, 382–403.

BRINDLEY, G. W., & WARDLE, R., 1970. Monoclinic and triclinic forms of pyrophyllite and pyrophyllite anhydride. *Am. Miner.* **55**, 1259–72.

BÜCHI, U. P., LEMCKE, K., WIENER, G., & ZIMDARS, J., 1965. Geologische Ergebnisse der Erdölexploration auf das Mesozoikum im Untergrund des schweizerischen Molassebeckens. *Bull. Verein. schweiz. Petrol.-Geol. u. -Ing.* **32**, 7–38.

BUDDINGTON, A. F., & LINDSLEY, D. H., 1964. Iron–titanium oxide minerals and synthetic equivalents. *J. Petrology*, **5**, 310–57.

CHATTERJEE, N. D., 1971. Phase equilibria in the Alpine metamorphic rocks of the environs of the Dora–Maira massif, western Italian Alps. *Neues Jb. Miner. Abh.* **114**, 181–245.

—— 1974*a*. X-Ray powder pattern and molar volume of synthetic 2M-paragonite: A Refinement. *Contr. Miner. Petrol.* **43**, 25–8.

—— 1974*b*. Synthesis and upper stability limit of 2M-margarite, $CaAl_2[Al_2Si_2O_{10}/(OH)_2]$. *Schweiz. miner. petrogr. Mitt.* **54**, 753–67.

—— & JOHANNES, W., 1974. Thermal stability and standard thermodynamic properties of synthetic $2M_1$-muscovite, $KAl_2[AlSi_3O_{10}(OH)_2]$. *Contr. Miner. Petrol.* **48**, 89–114.

CHENNAUX, G., & DUNOYER DE SEGONZAC, G., 1967. Etude pétrographique de la pyrophyllite du Silurien et du Dévonien au Sahara, répartition et origine. *Bull. Serv. Carte géol. Als. Lorr.* **20**, 195–210.

CLARK, S. P., & JÄGER, E., 1969. Denudation rate in the Alps from geochronologic and heat flow data. *Am. J. Sci.* **267**, 1143–60.

DICKSON, J. A. D., 1966. Carbonate identification and genesis as revealed by staining. *J. sedim. Petrol.* **36**, 491–505.

EUGSTER, H. P., & SKIPPEN, G. B., 1967. Igneous and metamorphic reactions involving gas equilibria. In ABELSON, P. H. (ed.), *Researches in geochemistry*, **2**. New York: John Wiley & Sons, 492–520.

FOX, J. S., 1974. Petrology of some low-variance meta-pelites from the Lukmanier Pass area, Switzerland. *Ph.D. thesis, Cambridge University*, 220 pp,

—— 1975. Three-dimensional isograds from the Lukmanier Pass, Switzerland, and their tectonic significance. *Geol. Mag.* **112**, 547–64.

FRENCH, B. W., 1966. Some geologic implications of equilibrium between graphite and a C–H–O gas phase at high temperatures and pressures. *Rev. Geophys.* **4**, 223–53.

FREY, J. D., 1967. Geologie des Greinagebietes (Val Camadra–Valle Cavalasca–Val di Larciolo–Passo della Greina). *Beitr. geol. Karte Schweiz, N.F.* **131**, 112 pp.

FREY, M., 1969*a*. Die Metamorphose des Keupers vom Tafeljura bis zum Lukmanier-Gebiet. *Ibid.* **137**, 160 pp,

—— 1969*b*. A mixed-layer paragonite/phengite of low-grade metamorphic origin. *Contr. Miner. Petrol.* **24**, 63–5.

—— & NIGGLI, E., 1971. Illit-Kristallinität, Mineralfazien und Inkohlungsgrad. *Schweiz. miner. petrogr. Mitt.* **51**, 229–34.

—— & ORVILLE, P. M., 1974. Plagioclase in margarite-bearing rocks. *Am. J. Sci.* **274**, 31–47.

GUIDOTTI, C. V., 1974. Transition from Staurolite to Sillimanite Zone. Rangeley Quadrangle, Maine. *Bull. geol. Soc. Am.* **85**, 475–90.

—— & SASSI, F. P., 1976. Muscovite as a petrogenetic indicator mineral in metamorphosed pelites and semipelites. *Neues Jb. Miner. Abh.*, **127**, 97–142.

HALFERDAHL, L. B., 1961. Chloritoid. Its composition, X-ray and optical properties, stability, and occurrence. *J. Petrology*, **2**, 49–135.

HANSEN, J. W., 1972. Zur Geologie, Petrographie und Geochemie der Bündnerschiefer-Serien zwischen Nufenenpass (Schweiz) und Cascate Toce (Italia). *Schweiz. miner. petrogr. Mitt.* **52**, 109–53.

HEIM, A., 1919. *Geologie der Schweiz. Band I: Molasseland und Juragebirge.* Leipzig: Tauchnitz.

HENDERSON, G. V., 1971. The origin of pyrophyllite–rectorite in shales of north central Utah. *Utah geol. mineral. Surv., Spec. Stud.* **34**, 37 pp.

HEWITT, D. A., 1973. Stability of the assemblage muscovite–calcite–quartz. *Am. Miner.* **58**, 785–91.

HEY, M. H., 1954. A new review of the chlorites. *Mineralog. Mag.* **30**, 277–92.

HOEFS, J., & FREY, M., 1976. The isotopic composition of carbonaceous matter in a metamorphic profile from the Swiss Alps. *Geochim. cosmochim. Acta*, **40**, 945–51.

HOLDAWAY, M. J., 1971. Stability of andalusite and the aluminum silicate phase diagram. *Am. J. Sci.* **271**, 97–131.

HOSCHEK, G., 1967. Untersuchungen zum Stabilitätsbereich von Chloritoid und Staurolith. *Contr. Miner. Petrol.* **14**, 123–62.

—— 1969. The stability of staurolite and chloritoid and their significance in metamorphism of pelitic rocks. *Ibid.* **22**, 208–32.

HUNZIKER, J. C., 1969. Rb–Sr-Altersbestimmungen aus den Walliser Alpen, Hellglimmer- und Gesamtgesteinsalterswerte. *Eclogae geol. Helv.* **62**, 527–42.

HSU, K. J., 1969. A preliminary analysis of the statics and kinetics of the Glarus overthrust. *Eclogae geol. Helv.* **62**, 143–54.

JÄGER, E., 1973: Die alpine Orogenase im Lichte der radiometrischen Altersbestimmung. *Eclogae geol. Helv.* **66**, 11–21.

JOHANNES, W., & ORVILLE, P. M., 1972. Zue Stabilität der Mineralparagenesen Muskovit + Calcit + Quarz, Zoisit + Muskovit + Quarz, Anorthit + K-Feldspat und Anorthit + Calcit. *Fortschr. Miner.* **50**, Beiheft **1**, 46–7.

KÖPPEL, V., & GRÜNENFELDER, M., 1975. Concordant U–Pb ages of monazite and xenotime from the Central Alps and the timing of the high temperature Alpine metamorphism, a preliminary report. *Schweiz. miner. petrogr. Mitt.* **55**, 129–32.

KÜBLER, B., 1967. La cristallinité de l'illite et les zones tout à fait supérieures du métamorphisme. In *Etages tectoniques*, Colloque à Neuchâtel, 105–22.

LANDIS, C. A., 1971. Graphitization of dispersed carbonaceous material in metamorphic rocks. *Contr. Miner. Petrol.* **30**, 30–45.

LIOU, J. G., 1971. *P–T* stabilities of laumontite, wairakite, lawsonite, and related minerals in the system $CaAl_2Si_2O_8$–SiO_2–H_2O. *J. Petrology*, **12**, 379–411.

LISZKAY, M., 1965. Geologie der Sedimentbedeckung das südwestlichen Gotthard-Massivs im Oberwallis. *Eclogae geol. Helv.* **58**, 901–65.

MACEWAN, D. M. C., RUIZ AMIL, A., & BROWN, G., 1961. Interstratified clay minerals. In BROWN, G. (ed.), *The X-ray Identification and Crystal Structures of Clay Minerals.* London: Miner. Soc., 393–445.

MAXWELL, D. T., & HOWER, J., 1967. High-grade diagenesis and low-grade metamorphism of illite in the Precambrian Belt Series. *Am. Miner.* **52**, 843–57.

MIYASHIRO, A., 1961. Evolution of metamorphic belts. *J. Petrology*, **2**, 277–311.

MULLIS, J., 1975. Growth conditions of quartz crystals from Val d'Illiez (Valais, Switzerland). *Schweiz. miner. petrogr. Mitt.* **55**, 419–29.

NEWTON, R. C., 1966. Kyanite–andalusite equilibrium from 700 to 800 °C. *Science*, **153**, 170–2.

NIGGLI, C. R., 1965. Petrographie und Petrogenesis der Migmatite und Gneise im südlichen Aarmassiv zwischen Obergesteln und Furkapass. *Ph.D. thesis, Bern University*, 115 pp.

NIGGLI, E., 1944. Das westliche Tavetscher Zwischenmassiv und der angrenzende Nordrand des Gotthardmassivs. *Schweiz. miner. petrogr. Mitt.* **24**, 58–301.

—— & NIGGLI, C., 1965. Karten der Verbreitung einiger Mineralien der alpidischen Metamorphose in den Schweizer Alpen (Stilpnomelan, Alkali-Amphibol, Chloritoid, Staurolith, Disthen, Sillimanit). *Eclogae geol. Helv.* **58**, 335–68.

NITSCH, K.-H., 1968. Die Stabilität von Lawsonit. *Naturwissenschaften*, **55**, 388.

—— & STORRE, B., 1972. Zur Stabilität von Margarit in H_2O–CO_2–Gasgemischen. *Fortschr. Miner.* **50**, Beiheft 1, 71–3.

PETERS, T., 1964. Tonmineralogische Untersuchungen an einem Keuper-Lias-Profil im Schweizer Jura (Frick). *Schweiz. miner. petrogr. Mitt.* **44**, 559–88.

—— 1965. Zur quantitativen röntgenographischen Bestimmung von Albit und Kalifeldspat in pelitischen Sedimentfraktionen. *Ibid.* **45**, 115–21.

—— 1970. A simple device to avoid orientation effects in X-Ray diffractometer samples. *Norelco Repr*, **17**, 23–4.

POTY, B., & STALDER, H. A., 1970. Kryometrische Bestimmungen der Salz- und Gasgehalte eingeschlossener Lösungen in Quarzkristallen aus Zerrklüften der Schweizer Alpen. *Schweiz. miner. petrogr. Mitt.* **50**, 141–54.

RICHARDSON, S. W., 1968. Staurolite stability in a part of the system Fe–Al–Si–O–H. *J. Petrology*, **9**, 467–88.

—— GILBERT, M., & BELL, P. M., 1969. Experimental determination of kyanite–andalusite and andalusite–sillimanite equilibria; the aluminum silicate triple point. *Am. J. Sci.* **267**, 259–72.

ROSENBERG, P. E., 1974. Pyrophyllite solid solutions in the system Al_2O_3–SiO_2–H_2O. *Am. Miner.* **59**, 254–60.

ROSENFELD, J. L., 1969. Stress effects around quartz inclusions in almandine and the piezothermometry of coexisting aluminum silicates. *Am. J. Sci.* **267**, 317–51.

SEKI, Y., 1959. Relation between chemical composition and lattice constants of epidote. *Am. Miner.* **44**, 720–30.

SHAW, D. M., 1956. Geochemistry of pelitic Rocks. Part III: Major elements and general geochemistry. *Bull. geol. Soc. Am.* **67**, 919–34.

STALDER, H. A., & TOURAY, J. C., 1970. Fensterquarze mit Methan-Einschlüssen aus dem westlichen Teil der schweizerischen Kalkalpen. *Schweiz. miner. petrogr. Mitt.* **50**, 109–30.

STORRE, B., & NITSCH, K.-H., 1974. Zur Stabilität von Margarit im System CaO–Al_2O_3–SiO_2–H_2O. *Contr. Miner. Petrol.* **43**, 1–24.

SWEATMAN, T. R., & LONG, J. V. P., 1969. Quantitative electron-probe microanalysis of rock-forming minerals. *J. Petrology*, **10**, 332–79.

TANK, R. W., & MCNEELY, L., 1970. Clay minerals associated with the Precambrian Gowganda Formation of Ontario. *Clay Minerals*, **8**, 471–7.

THOMPSON, A. B., 1970*a*. A note on the kaolinite–pyrophyllite equilibrium *Am. J. Sci.* **268**, 454–8.

—— 1970*b*. Laumontite equilibria and the zeolite facies. *Ibid.* **269**, 267–75.

TOURAY, J. C., VOGLER, M., & STALDER, H. A., 1970. Inclusions à hydrocarbures liquéfiés dans les quartz de Zingel/Seewen (Suisse). *Schweiz. miner. petrogr. Mitt.* **50**, 131–9.

TRUMPY, R., 1949. Der Lias der Glarner Alpen. *Denkschr. schweiz. natf. Ges.* **79**, 192 pp.

—— 1960. Palaeotectonic evolution of the Central and Western Alps. *Bull. geol. Soc. Am.* **71**, 843–908.

—— 1969. Die helvetischen Decken der Ostschweiz: Versuch einer palinspastischen Korrelation und Ansätze zu einer kinematischen Analyse. *Eclogae geol. Helv.* **62**, 105–42.

VELDE, B., 1971. The stability and natural occurrence of margarite. *Miner. Mag.* **38**, 317–23.

VINE, J. D., & TOURTELOT, E. B., 1970. Geochemistry of black shale deposits—A Summary Report. *Econ. Geol.* **65**, 253–72.

VINOGRADOV, A. P., & RONOV, A. B., 1956. Evolution of the chemical composition of clays of the Russian platform. *Geochem. int.* **2**, 123–39.

WARSHAW, C. M., & ROY, R., 1961. Classification and a scheme for the identification of layer silicates. *Bull. geol. Soc. Am.* **72**, 1455–92.

WETZEL, R., 1973. Chemismus und physikalische Parameter einiger Chlorite aus der Grünschieferfazies. *Schweiz. miner. petrogr. Mitt.* **53**, 273–98.

WINCHELL, H., 1958. The composition and physical properties of garnet. *Am. Miner.* **43**, 595–600.

ZEN, E-AN, 1960. Metamorphism of Lower Paleozoic rocks in the vicinity of the Taconic range in west-central Vermont. *Ibid.* **45**, 129–75.